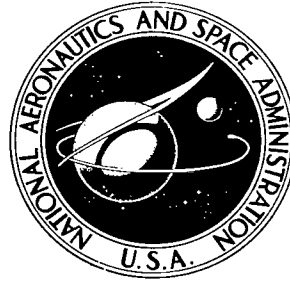


NASA TECHNICAL NOTE



NASA TN D-6002

e.1

NASA TN D-6002

LOAN COPY: RETURN TO
AFWL (DOGL)
KIRTLAND AFB, NM



EFFECTS OF A RETROROZZLE LOCATED AT
THE APEX OF A 140° BLUNT CONE AT
MACH NUMBERS OF 3.00, 4.50, AND 6.00

by Robert J. McGhee
Langley Research Center
Hampton, Va. 23365



ERRATA

NASA Technical Note D-6002

EFFECTS OF A RETRINOZZLE LOCATED AT THE APEX
OF A 140° BLUNT CONE AT MACH NUMBERS
OF 3.00, 4.50, and 6.00

By Robert J. McGhee
January 1971

Page 24: Figure 4(f) was printed incorrectly and should be replaced by the attached corrected figure.

Issue date: January 1971

NATIONAL AERONAUTICS AND SPACE ADMINISTRATION
WASHINGTON, D. C. 20546
OFFICIAL BUSINESS

FIRST CLASS MAIL



POSTAGE AND FEES PAID
NATIONAL AERONAUTICS AND
SPACE ADMINISTRATION

05U 001 26 51 3DS 71012 00903
AIR FORCE WEAPONS LABORATORY /WLOL/
KIRTLAND AFB, NEW MEXICO 87117

ATT E. LOU BOWMAN, CHIEF, TECH. LIBRARY

POSTMASTER: If Undeliverable (Section 158
Postal Manual) Do Not Return



0132755

1. Report No. NASA TN D-6002	2. Government Accession No.	3. Recipient's Catalog No.	
4. Title and Subtitle EFFECTS OF A RETRINOZZLE LOCATED AT THE APEX OF A 140° BLUNT CONE AT MACH NUMBERS OF 3.00, 4.50, AND 6.00		5. Report Date January 1971	
		6. Performing Organization Code	
7. Author(s) Robert J. McGhee		8. Performing Organization Report No. L-7312	
9. Performing Organization Name and Address NASA Langley Research Center Hampton, Va. 23365		10. Work Unit No. 126-13-10-22	
		11. Contract or Grant No.	
12. Sponsoring Agency Name and Address National Aeronautics and Space Administration Washington, D.C. 20546		13. Type of Report and Period Covered Technical Note	
		14. Sponsoring Agency Code	
15. Supplementary Notes			
16. Abstract Several distinct types of flow occurred on the cone, including two unsteady-flow regimes and two steady-flow regimes. Generally, the unsteady flows were restricted to low values of nozzle thrust and were observed at all angles of attack. The two steady-flow regimes occurred with increasing nozzle thrust; at the highest test values of nozzle thrust, the condition of no shear-layer reattachment on the cone was approximated. For the steady-flow regimes, the locations of the jet shock, flow interface, and bow shock together with the separation and reattachment pressures were all primarily functions of the nozzle-thrust coefficient. Because of the extensive flow separation and accompanying low pressure on the cone surface, only at the highest thrust values was the total drag (integrated-pressure drag coefficient plus nozzle-thrust coefficient) greater than the jet-off value of integrated-pressure drag coefficient. This result was obtained at all three test Mach numbers.			
17. Key Words (Suggested by Author(s)) Blunt cone Jet-plume effects Flow separation		18. Distribution Statement Unclassified - Unlimited	
19. Security Classif. (of this report) Unclassified	20. Security Classif. (of this page) Unclassified	21. No. of Pages 38	22. Price* \$ 3.00

EFFECTS OF A RETRINOZZLE LOCATED AT THE APEX

OF A 140° BLUNT CONE AT MACH NUMBERS

OF 3.00, 4.50, AND 6.00

By Robert J. McGhee
Langley Research Center

SUMMARY

Some effects of a supersonic retronozzle located at the apex of a 140° spherically blunted cone have been investigated at free-stream Mach numbers of 3.00, 4.50, and 6.00 at angles of attack of 0° , 2° , and 5° . Nozzle thrust was varied over a large range, and surface-pressure distributions and schlieren photographs were obtained. The free-stream Reynolds number varied from about 0.7×10^6 to 1.0×10^6 per foot (2.3×10^6 to 3.3×10^6 per meter) as the Mach number was increased from 3.00 to 6.00.

Several distinct types of flow occurred on the cone, including two unsteady-flow regimes and two steady-flow regimes. Generally, the unsteady flows were restricted to low values of nozzle thrust and were observed at all angles of attack. The two steady-flow regimes occurred with increasing nozzle thrust; at the highest test values of nozzle thrust, the condition of no shear-layer reattachment on the cone was approximated. For the steady-flow regimes, the locations of the jet shock, flow interface, and bow shock together with the separation and reattachment pressures were all primarily functions of the nozzle-thrust coefficient. Because of the extensive flow separation and accompanying low pressures on the cone surface, only at the highest thrust values was the total drag (integrated-pressure drag coefficient plus nozzle-thrust coefficient) greater than the jet-off value of integrated-pressure drag coefficient. This result was obtained at all three test Mach numbers.

INTRODUCTION

The use of retrorockets located on the surface of conical aeroshells is one system that may be considered for braking vehicles during their descent through a planetary atmosphere. The use of this type of system requires an understanding of the flow field that results from interaction of retrorocket exhaust with oncoming flow and of the subsequent effects on the entry vehicle.

Reference 1 presents exploratory results in the form of high-speed motion pictures and schlieren photographs to illustrate the effect of forward-facing jets on the bow shock of a blunt body in a Mach 6 free stream for low values of jet-total-pressure ratio. References 2 and 3 present pressure results for forward-facing jets below a Mach number of 3 for flat-faced cylindrical bodies and a blunt body. References 4 to 6 present pressure and force results obtained for blunt bodies with single- and multiple-nozzle configurations.

The present investigation was initiated to study the interaction of a single supersonic jet exhausting from a conical aeroshell. Most of the previous tests were performed for jet flow exhausting from tubes or flat-faced cylinders and do not reflect the interactions of interest for planetary entry vehicles. This investigation also provides experimental results which are very helpful in the development of analytical methods to predict the flow field in the immediate vicinity of a planetary entry vehicle employing retro-rockets. Results were obtained for a single supersonic retronozzle located at the apex of a 140° blunt cone for high jet-total-pressure ratios and for Mach numbers from 3.00 to 6.00. Surface-pressure distributions and schlieren photographs were obtained at angles of attack of 0° , 2° , and 5° .

SYMBOLS

C_D	drag coefficient, from integrated pressures at $\alpha = 0^\circ$
C_p	pressure coefficient, $\frac{p - p_\infty}{q_\infty}$
C_T	nozzle-thrust coefficient, $\frac{T}{q_\infty S}$
D_b	cone-base diameter
D_n	cone-nose diameter
d_e	nozzle-exit diameter
H	distance to flow interface (see fig. 11)
h	jet-shock standoff distance (see fig. 10)
l	bow-shock standoff distance at jet-on conditions at $\alpha = 0^\circ$ (see fig. 12)
M	Mach number

p	static pressure
p _t	total pressure
q	dynamic pressure
r	local radius measured from cone center line
S	model base area, 0.11 ft ² (102.19 cm ²)
T	nozzle thrust, $\frac{\pi d_e^2}{4} (2q_j + p_j - p_\infty)$
α	angle of attack
δ	bow-shock standoff distance at jet-off conditions at $\alpha = 0^\circ$ (see fig. 7)

Subscripts:

j	jet
s	separation (conditions at orifice 1)
r	reattachment
∞	free stream

APPARATUS AND TESTS

Model

A sketch of the general arrangement of the test model, sting, and nozzle is shown in figure 1, and model details, nozzle details, and orifice locations are shown in figure 2.

The 140° cone model had a spherical nose bluntness D_n/D_b of 0.50 with a supersonic retronozzle located at the apex. The cone had a sharp shoulder, and the base diameter D_b was 4.50 inches (11.43 cm). Twelve static-pressure orifices (0.06 inch (0.15 cm) in diameter) drilled perpendicular to the local-surface slope were located along a ray on the upper half of the model (see fig. 2).

The model support sting was made of a hollow steel tube to allow gaseous nitrogen from a supply tank to empty into a plenum ahead of the nozzle (see fig. 1). The area

ratio of the nozzle (ratio of exit area to throat area) was 4.24, and the design Mach number for one-dimensional isentropic flow was 3.00. Cold, gaseous nitrogen at approximately local atmospheric total temperature (70° F (294° K)) was used to obtain the exhaust plume. The nozzle was sized to obtain test data up to a thrust coefficient of about 2.

Wind Tunnel

The tests were conducted in a 2-foot hypersonic facility at the Langley Research Center. This wind tunnel, described in reference 7, is an ejector type which provides continuous flow at high Mach numbers and low densities. The average conditions for the present investigation are shown in the following table:

M _∞	Stagnation temperature		Stagnation pressure		Dynamic pressure		Static pressure		Reynolds number	
	°F	°K	lb/ft ²	kN/m ²	lb/ft ²	kN/m ²	lb/ft ²	kN/m ²	per ft	per m
3.00	100	311	696	33	119.36	5.71	18.95	0.91	0.71 × 10 ⁶	2.33 × 10 ⁶
4.50	300	422	2949	141	144.43	6.92	10.19	.49	.87	2.85
6.00	300	422	6129	293	97.82	4.68	3.88	.19	.99	3.25

Nitrogen Supply

High-pressure gaseous nitrogen was generated by pumping liquid nitrogen to the required storage pressure and converting it from liquid to gas in a steam-actuated heat exchanger. The high-pressure gaseous nitrogen was then stored in a tank farm having a capacity of 800 ft³ (22.65 m³). Suitable pressure-reducing and pressure-regulating valves were remotely controlled to obtain the nitrogen gas pressure in a manifold outside the test section which, in turn, fed the nozzle plenum chamber in the model. Once the correct pressure was obtained in the manifold, a quick-acting guillotine valve was employed to initiate and terminate the flow to the nozzles. Minor pressure adjustments could be made after initiation of flow through the nozzles.

Instrumentation

The local-cone-surface pressures and the nozzle-plenum pressure were obtained from absolute pressure-measuring transducers. Data were obtained by a high-speed data acquisition system and recorded on magnetic tape. Schlieren photographs were obtained with the use of a 2-μsec flash from a xenon light source.

Tests and Accuracy

Pressure and schlieren data were obtained at free-stream Mach numbers of 3.00, 4.50, and 6.00 at angles of attack of 0° , 2° , and 5° . Since the pressure orifices were located only on the upper surface of the model, the pressure data obtained at $\alpha = -2^\circ$ and -5° are plotted at negative values of r/D_b for $\alpha = 2^\circ$ and 5° in figures 3 to 5. The range of $p_{t,j}/p_{t,\infty}$ varied from jet off to about 250, 70, and 20 at free-stream Mach numbers of 3.00, 4.50, and 6.00, respectively. The surface of the model was smooth; that is, no boundary-layer transition strips were employed, and it is believed that laminar flow existed over the entire model surface at jet-off conditions since the model length was small and the test Reynolds numbers were low.

The maximum Mach number variation in the region of the test model was less than ± 0.04 , and the angles of attack were accurate to within $\pm 0.1^\circ$. Accuracy of the pressure transducers was better than 1 percent of the full-scale range of the gage (2.0 lb/in² (13.8 kN/m²)). The repeatability of the data is indicated in several figures (see figs. 3 to 5). The values of $p_{t,j}/p_{t,\infty}$ quoted herein are estimated to be accurate within ± 2 percent.

RESULTS AND DISCUSSION

Surface-pressure data and schlieren photographs are presented in figures 3 to 5 to illustrate the effects of angle of attack and Mach number for varying jet-total-pressure ratio. Figures 6 and 7 present the effect of Mach number on the surface-pressure coefficient and bow-shock standoff distance for jet-off conditions and $\alpha = 0^\circ$. The various flow regimes that occurred in the test program are illustrated by the schlieren photographs in figure 8, and figure 9 illustrates the flow phenomena induced by the jet. Figures 10 to 12 present the jet-shock location, flow-interface location, and bow-shock location as functions of Mach number and thrust coefficient. In figure 13, the pressure coefficients at separation and reattachment are shown as functions of Mach number and thrust coefficient. The measured surface pressures were integrated to obtain the drag coefficients at $\alpha = 0^\circ$, and these integrated-pressure drag coefficients are presented as functions of Mach number and thrust coefficient in figure 14.

Jet-Off Aerodynamics

Pressure coefficients presented in figures 3 to 5 were obtained at angles of attack of 0° , 2° , and 5° . The pressure coefficients for jet-off conditions were higher on the windward surface (negative r/D_b) than on the leeward surface (positive r/D_b) at angles of attack of 2° and 5° , as expected. Figure 6 indicates the effects on C_p of free-stream Mach number for $\alpha = 0^\circ$. Values of C_p at $r/D_b = 0$ were calculated from

normal-shock equations, since no data were obtainable because of the nozzle location. These calculated values are denoted in figure 6 by solid symbols. The increase in the pressure-coefficient data with an increase in M_∞ from 3.00 to 6.00 is similar to the trend of the calculated values. At $M_\infty = 4.50$, however, the pressure coefficients generally were less than those at $M_\infty = 3.00$. This result is not understood at present, but a possible explanation is indicated by the schlieren photographs of figure 4, which show weak shock waves from the tunnel nozzle near the cone at $M_\infty = 4.50$. Other characteristics at $M_\infty = 4.50$ appear to have the correct magnitudes, as shown subsequently.

Bow-shock standoff distances referred to the virtual apex of the 140° blunt cone are shown in figure 7 as functions of Mach number. For comparison, the bow-shock standoff distances obtained from the theory of reference 8 are shown for a 140° sharp cone. Both the trend with Mach number and the magnitude of the measured distances are in reasonable agreement with the theory. This agreement suggests that for the amount of blunting ($\frac{D_n}{D_b} = 0.50$), the bow-shock standoff distance is primarily a function of cone semiapex angle.

Jet-On Aerodynamics

Flow observations. - From a study of the schlieren photographs in figures 3 to 5 and other schlieren photographs obtained in this investigation, four different flow regimes were observed at $\alpha = 0^\circ$. Similar flow regimes have been observed in other investigations (refs. 1 and 2), but as far as is known, this is the first observation of all four flow regimes during a single investigation. The types of flow that existed were found to be primarily functions of nozzle-exit characteristics (for a fixed-nozzle-geometry thrust coefficient). The four flow regimes are identified in figure 8 and related to C_T .

For $C_T = 0.03$ (regime 1; $p_j < p_s$), the flow penetrated forward a short distance from the nozzle exit and the flow field was unsteady. For this regime the local pressure in the vicinity of the nozzle exit was greater than the jet-exit static pressure would be if the nozzle flow were fully expanded, and some flow separation in the nozzle itself probably occurred. The resulting flow unsteadiness is probably related to the unsteady character of the nozzle boundary-layer separation and its effect on the exhaust flow. For $C_T = 0.11$ (regime 2; $p_j \approx p_s$), the jet flow penetrated far upstream and the flow field was unsteady. For this flow regime the local pressure in the vicinity of the nozzle exit was approximately equal to the jet-exit static pressure, the nozzle flow being fully expanded. For $C_T = 0.32$ (regime 3; $p_j > p_s$), the upstream penetration of the jet flow decreased and the flow field was steady. For this regime the nozzle flow was highly underexpanded. Flow reattachment occurred on the outer periphery of the cone. An increase to $C_T = 1.60$ (regime 4; $p_j > p_s$) caused the steady flow field to become large with respect to the nozzle-exit diameter, and the cone was immersed in the wake of the jet flow. Regime 4

has been identified in the literature as the flow regime where the body is completely immersed in a wake-type flow with no shear-layer reattachment occurring on the body (e.g., ref. 9). The schlieren photographs indicate that the condition of no shear-layer reattachment is approximated at the cone shoulder.

A schlieren photograph and a sketch of regime 3 are presented in figure 9 to illustrate the features of the flow fields. (Descriptions of these flow phenomena are given in ref. 1.) Flow phenomena such as the separated-flow region, the jet shock, the interface, and the reattachment shock are shown. The nozzle flow expands from the supersonic exhaust velocity at the nozzle-exit plane to some much higher Mach number, experiences a strong terminal shock and then decelerates subsonically to a mutual stagnation point along the axis, and turns and flows downstream. The oncoming free-stream flow encounters a bow shock, and the recovered stagnation pressure for both flows must be equal. An interface which appears as a thin region in which viscous forces are strong separates the free-stream flow from the nozzle flow. The oncoming free-stream flow undergoes a sudden deceleration and entropy increase through the bow-shock wave and then turns subsonically and flows outward between the bow-shock wave and the interface with a subsequent reacceleration to sonic and supersonic velocities, while the nozzle flow which passes through the jet shock flows outward between the jet shock and the interface. Viscous interaction and mixing between the two gas streams occurs along the interface. The region of separated flow, or dead-air region (recirculation region), is bounded by the cone surface, the jet boundary, and the mixed-flow region, with flow reattachment occurring near the cone shoulder.

Jet shock, flow interface, and bow-shock location at $\alpha = 0^\circ$. - Figures 10 to 12 present the jet-shock, flow-interface, and bow-shock locations as functions of nozzle-thrust coefficient. The jet-shock location is related to the diameter of the nozzle exit, and the flow-interface and bow-shock locations are related to the diameter of the cone base. These locations were measured from the schlieren photographs taken during the investigation. Increasing the nozzle-thrust coefficient C_T in the steady-flow regimes results in a forward movement of the jet-shock, flow-interface, and bow-shock locations. The jet-shock location can be seen in figure 10 to be largely dependent on C_T with little dependence upon free-stream Mach number. Both the interface and bow-shock locations (figs. 11 and 12) are also strongly influenced by C_T ; however, some Mach number dependency is indicated for the bow-shock location, as would be expected.

Correlation of pressure data at $\alpha = 0^\circ$. - The separation pressure coefficient (at orifice 1) and the pressure coefficient at flow reattachment are presented in figure 13 as functions of C_T for $\alpha = 0^\circ$. In general, both the separation and reattachment

pressures were correlated by C_T in the steady-flow regime and do not show obvious dependence on any other variables.

Effect of integrated-pressure drag coefficient. - Integrated-pressure drag coefficients at $\alpha = 0^\circ$ are presented in figure 14 as functions of C_T . The integrated-pressure drag coefficient on the cone C_D (see solid symbols) decreased with increasing C_T ; this decrease in C_D is associated with the low pressures on the cone surface in the separated-flow region. Integrated-pressure drag coefficient plus nozzle-thrust coefficient $C_D + C_T$ (see open symbols) also initially decreased with increasing C_T (in the unsteady regimes), and a value of $C_T \gtrsim 1.60$ is required to obtain a value of $C_D + C_T$ equal to the C_D alone at jet-off conditions. This result was obtained at all three test Mach numbers. Reference 6 indicates that for C_T above about 2, there is little difference between the total drag ($C_D + C_T$) and the thrust coefficient of the jet alone (C_T) for a 120° blunt cone at $M_\infty = 2.0$.

Effect of angle of attack. - Regions of unsteady flow, similar in character to those for $\alpha = 0^\circ$ previously discussed, were observed at angles of attack of 2° and 5° by inspection of the schlieren photographs (figs. 3 to 5) at all test Mach numbers and low test values of $p_{t,j}/p_{t,\infty}$. At high test values of $p_{t,j}/p_{t,\infty}$ large regions of flow separation and low pressure coefficients occurred on the leeward surface; somewhat larger pressure coefficients occurred on the windward surface, with flow reattachment occurring near the shoulder of the cone. In the unsteady-flow regimes, surface-pressure coefficients larger than jet-off values occurred on the windward surface at $\alpha = 2^\circ$ and 5° . The results of reference 10 also indicate reattachment pressures higher than stagnation pressure for a 120° blunt cone with a sharp cone-cylinder spike located at the apex.

CONCLUDING REMARKS

Some effects of a supersonic retronozzle located at the apex of a 140° spherically blunted cone have been investigated at free-stream Mach numbers of 3.00, 4.50, and 6.00 at angles of attack of 0° , 2° , and 5° . Nozzle thrust was varied over a large range, and surface-pressure distributions and schlieren photographs were obtained. The free-stream Reynolds number varied from about 0.7×10^6 to 1.0×10^6 per foot (2.3×10^6 to 3.3×10^6 per meter) as the Mach number was increased from 3.00 to 6.00.

Several distinct types of flow occurred on the cone, including two unsteady-flow regimes and two steady-flow regimes. Generally, the unsteady flows were restricted to low values of nozzle thrust and were observed at all angles of attack. The two steady-flow regimes occurred with increasing nozzle thrust; at the highest test values of nozzle thrust, the condition of no shear-layer reattachment on the cone was approximated. For the steady-flow regimes, the locations of the jet shock, flow interface, and bow shock

together with the separation and reattachment pressures were all primarily functions of the nozzle-thrust coefficient. Because of the extensive flow separation and accompanying low pressures on the cone surface, only at the highest thrust values was the total drag (integrated-pressure drag coefficient plus nozzle-thrust coefficient) greater than the jet-off value of integrated-pressure drag coefficient. This result was obtained at all three test Mach numbers.

Langley Research Center,
National Aeronautics and Space Administration,
Hampton, Va., August 7, 1970.

REFERENCES

1. Romeo, David J.; and Sterrett, James R.: Exploratory Investigation of the Effect of a Forward-Facing Jet on the Bow Shock of a Blunt Body in a Mach Number 6 Free Stream. NASA TN D-1605, 1963.
2. Hayman, Lovick O., Jr.; and McDearmon, Russell W.: Jet Effects on Cylindrical Afterbodies Housing Sonic and Supersonic Nozzles Which Exhaust Against a Supersonic Stream at Angles of Attack From 90° to 180° . NASA TN D-1016, 1962.
3. Charczenko, Nickolai; and Hennessey, Katherine W.: Investigation of a Retrorocket Exhausting From the Nose of a Blunt Body Into a Supersonic Free Stream. NASA TN D-751, 1961.
4. Peterson, Victor L.; and McKenzie, Robert L.: Effects of Simulated Retrorockets on the Aerodynamic Characteristics of a Body of Revolution at Mach Numbers From 0.25 to 1.90. NASA TN D-1300, 1962.
5. Keyes, J. Wayne; and Hefner, Jerry N.: Effect of Forward-Facing Jets on Aerodynamic Characteristics of Blunt Configurations at Mach 6. J. Spacecraft Rockets, vol. 4, no. 4, Apr. 1967, pp. 533-534.
6. Jarvinen, Philip O.; and Adams, Richard H.: The Effects of Retrorockets on the Aerodynamic Characteristics of Conical Aeroshell Planetary Entry Vehicles. AIAA Pap. No. 70-219, Jan. 1970.
7. Stokes, George M.: Description of a 2-Foot Hypersonic Facility at the Langley Research Center. NASA TN D-939, 1961.
8. Campbell, James F.: Supersonic Aerodynamic Characteristics and Shock Standoff Distances for Large-Angle Cones With and Without Cylindrical Afterbodies. NASA TN D-5334, 1969.
9. Jarvinen, Philip O.; Luce, Richard W.; and Wachslar, Emmanuel: Propulsive Re-Entry Aerodynamics. MC 68-3001-R1 (BNY) (Contract No. NAS 7-576), MITHRAS, June 1968.
10. McGhee, Robert J.; and Staylor, W. Frank: Aerodynamic Investigation of Sharp Cone-Cylinder Spikes on 120° Blunted Cones at Mach Numbers of 3.00, 4.50, and 6.00. NASA TN D-5201, 1969.

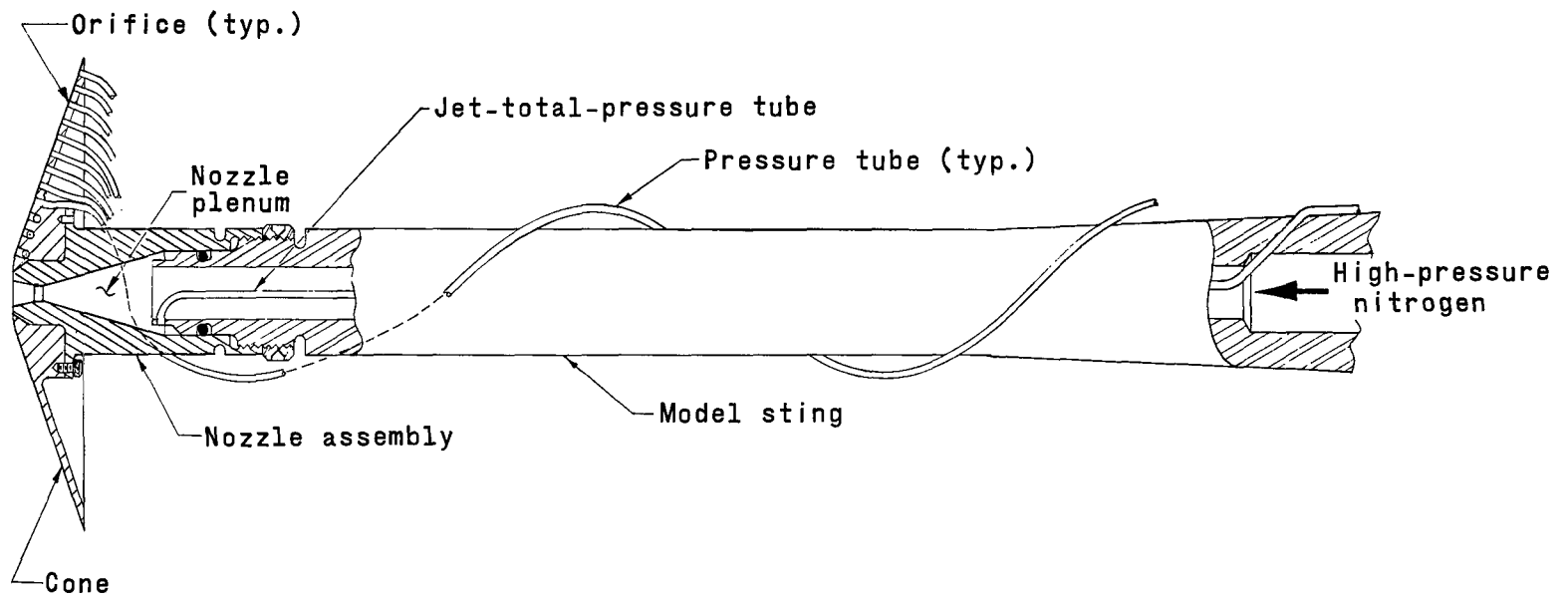
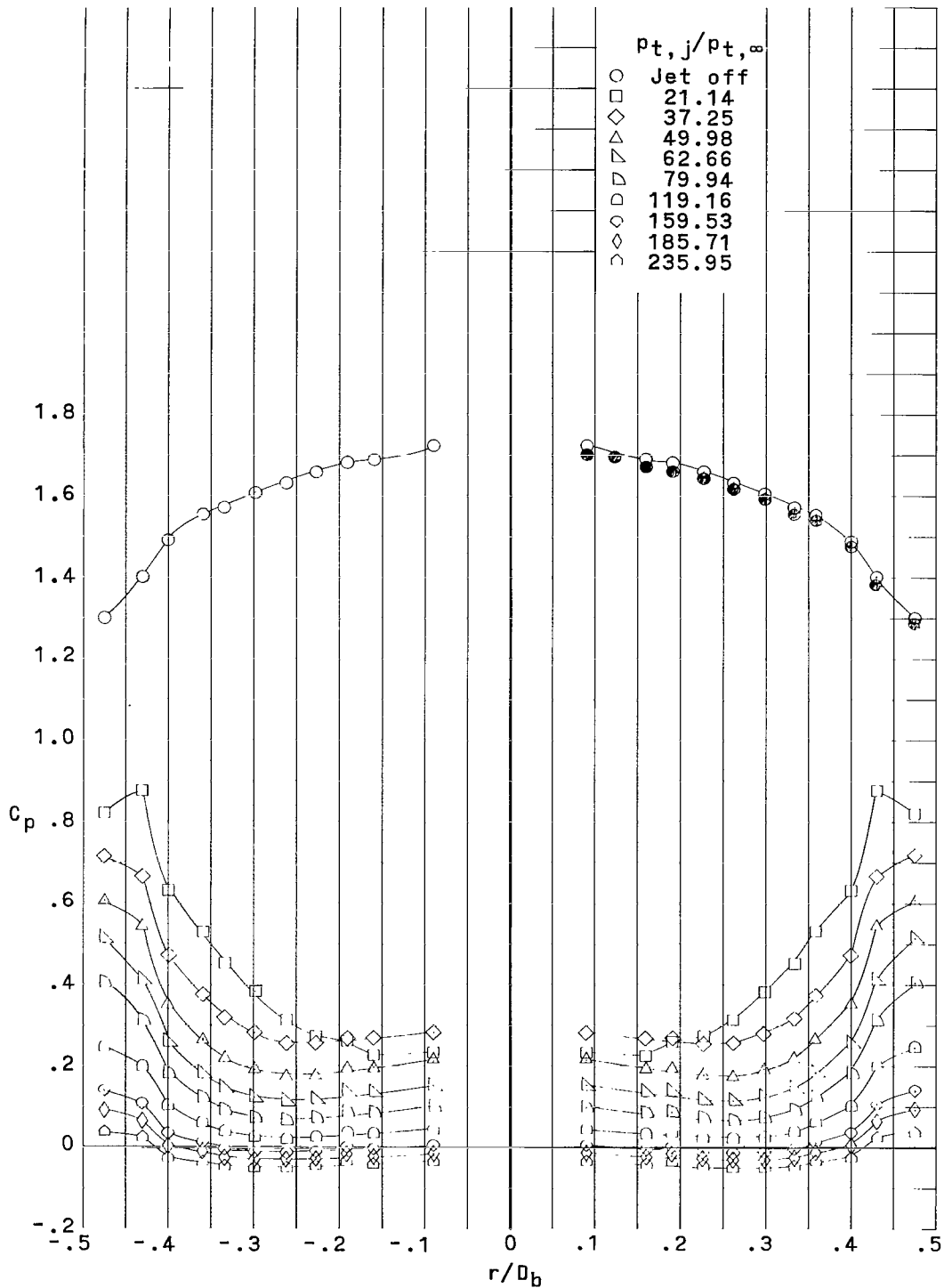
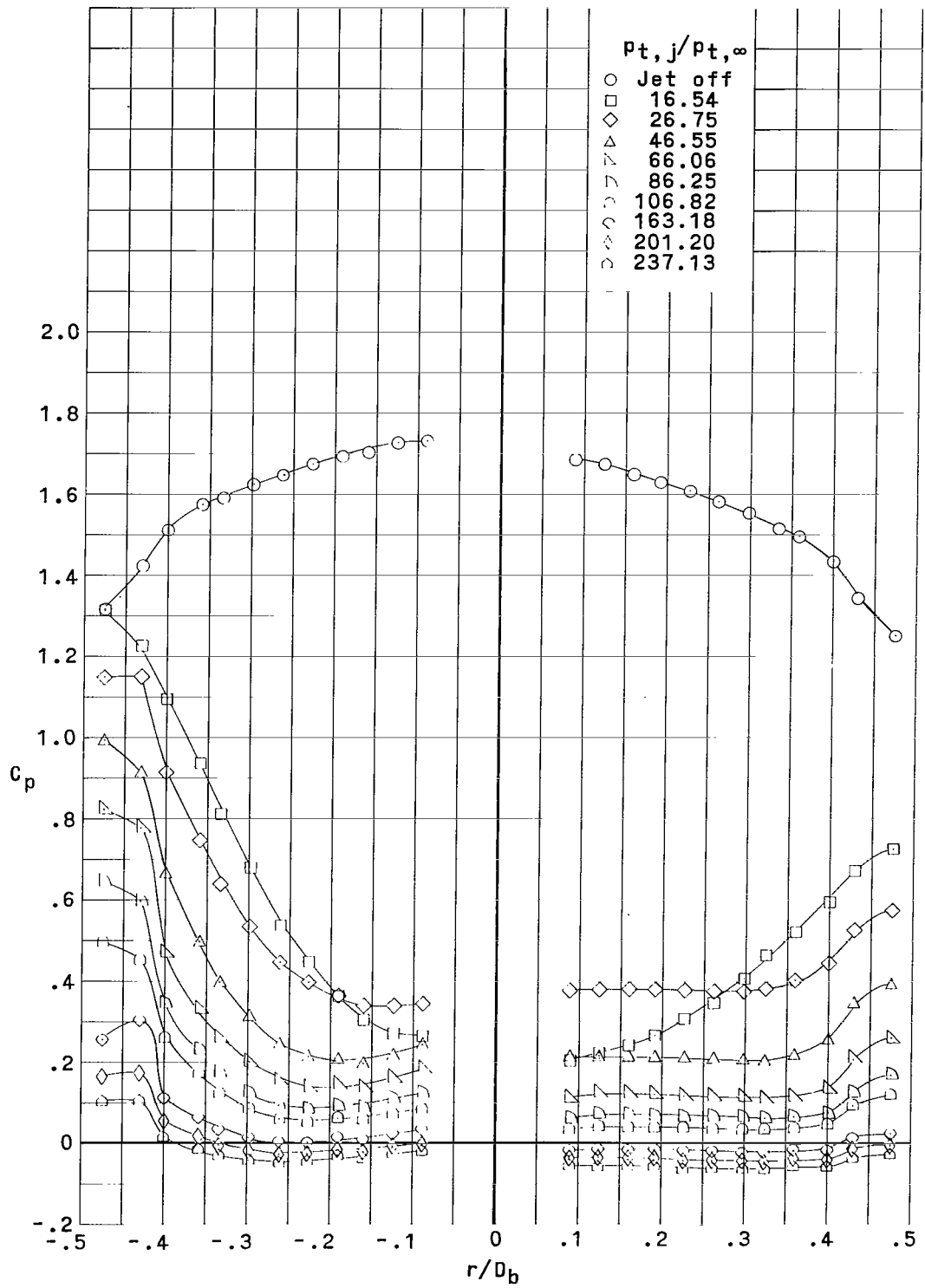


Figure 1.- Sketch of cone showing sting and nozzle arrangement.



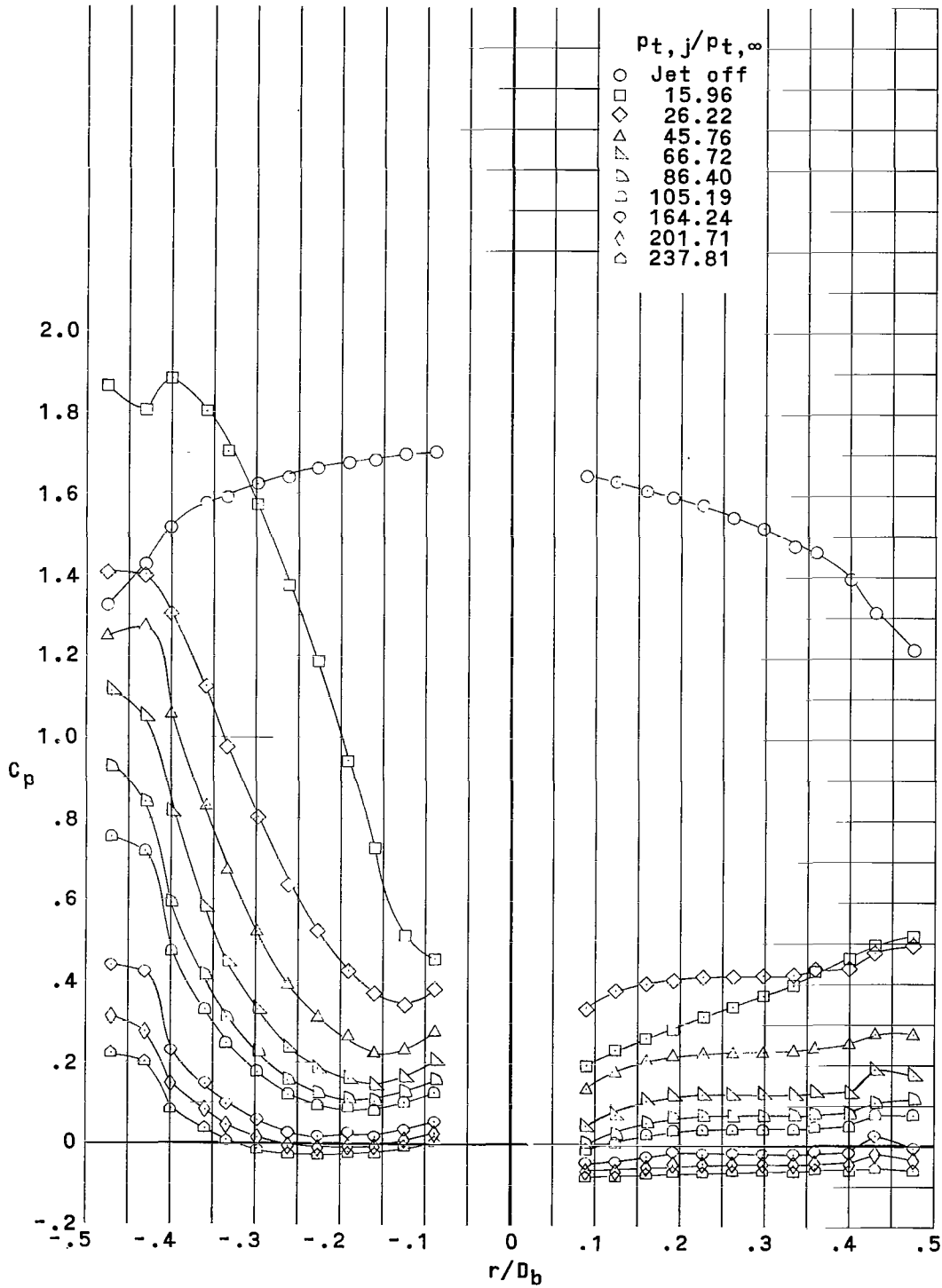
(a) Pressure distribution at $\alpha = 0^\circ$.

Figure 3.- Pressure distributions and schlieren photographs for varying $P_{t,j}/P_{t,\infty}$. $M_\infty = 3.00$. (Solid symbols indicate repeat data.)



(b) Pressure distribution at $\alpha = 2^\circ$.

Figure 3.- Continued.



(c) Pressure distribution at $\alpha = 5^\circ$.

Figure 3.- Continued.



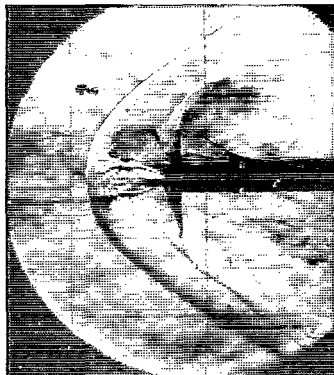
Jet off



$p_{t,j}/p_{t,\infty}=21.14$



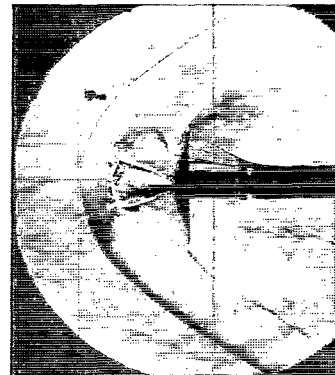
$p_{t,j}/p_{t,\infty}=37.25$



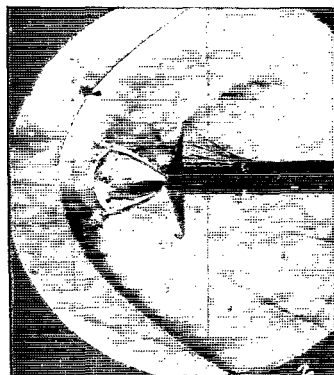
$p_{t,j}/p_{t,\infty}=49.98$



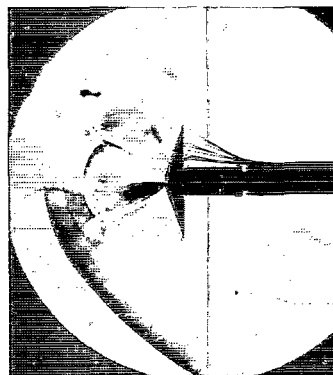
$p_{t,j}/p_{t,\infty}=62.66$



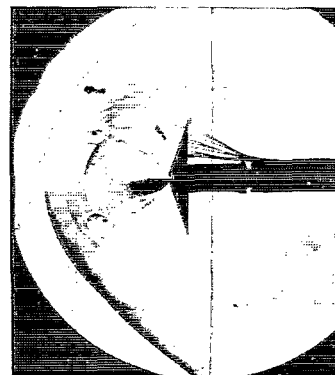
$p_{t,j}/p_{t,\infty}=79.94$



$p_{t,j}/p_{t,\infty}=119.16$



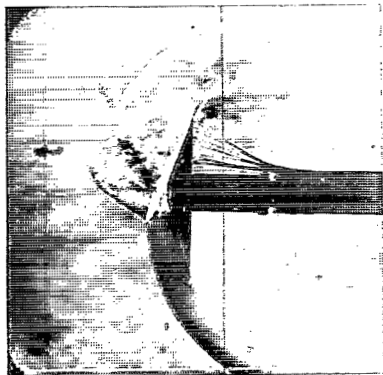
$p_{t,j}/p_{t,\infty}=169.20$



$p_{t,j}/p_{t,\infty}=185.71$

(d) Schlieren photographs at $\alpha = 0^\circ$. L-70-4747

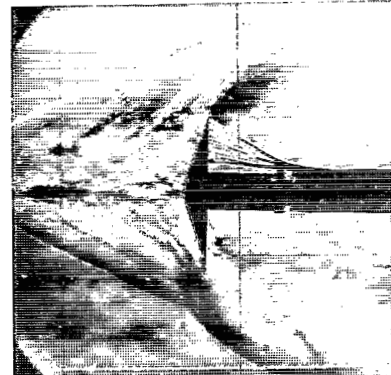
Figure 3.- Continued.



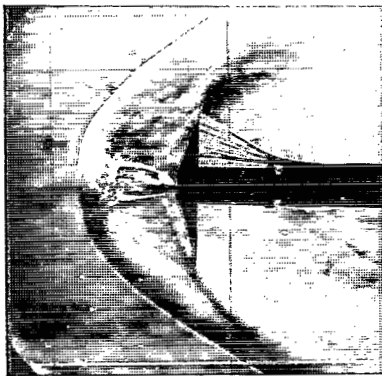
$p_{t,j}/p_{t,\infty}=6.82$



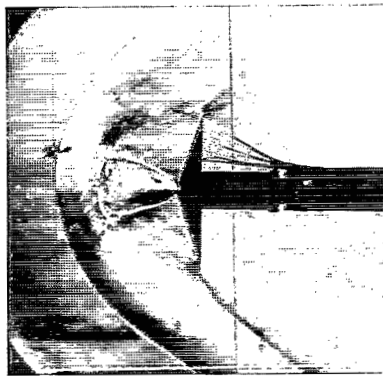
$p_{t,j}/p_{t,\infty}=11.35$



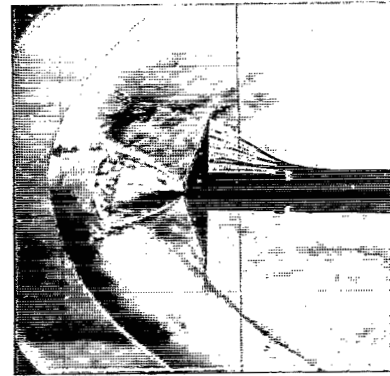
$p_{t,j}/p_{t,\infty}=16.54$



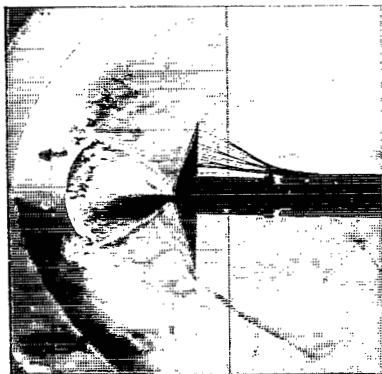
$p_{t,j}/p_{t,\infty}=46.55$



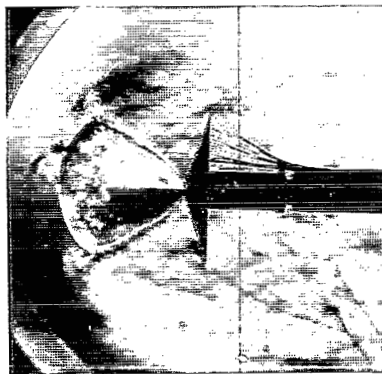
$p_{t,j}/p_{t,\infty}=86.25$



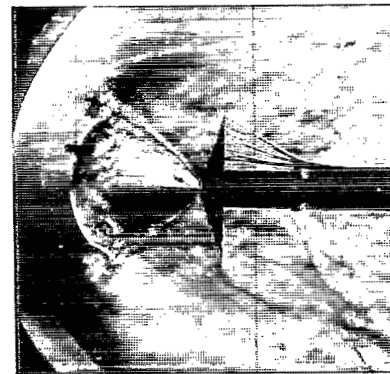
$p_{t,j}/p_{t,\infty}=106.82$



$p_{t,j}/p_{t,\infty}=163.18$



$p_{t,j}/p_{t,\infty}=237.13$



$p_{t,j}/p_{t,\infty}=252.16$

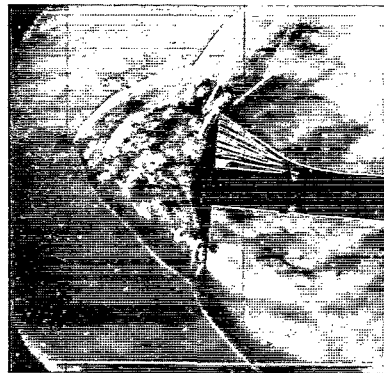
(e) Schlieren photographs at $\alpha = 2^\circ$.

L-70-4748

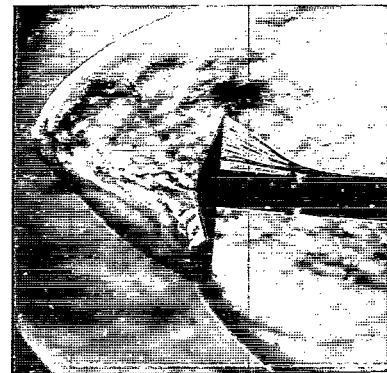
Figure 3.- Continued.



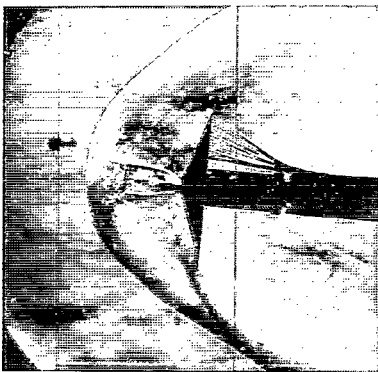
Jet off



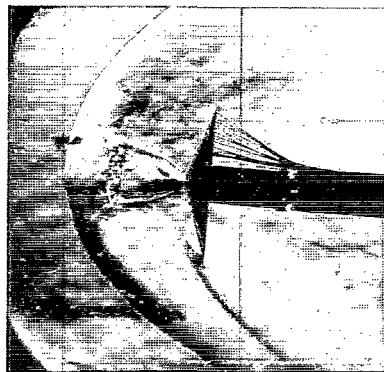
$p_{t,j}/p_{t,\infty}=6.71$



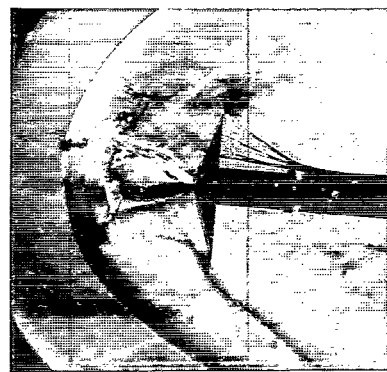
$p_{t,j}/p_{t,\infty}=15.96$



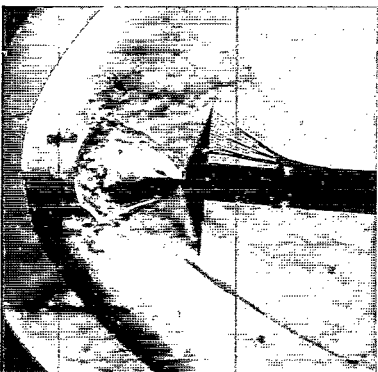
$p_{t,j}/p_{t,\infty}=45.76$



$p_{t,j}/p_{t,\infty}=86.40$



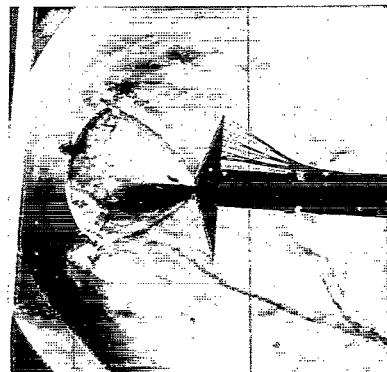
$p_{t,j}/p_{t,\infty}=105.19$



$p_{t,j}/p_{t,\infty}=164.24$



$p_{t,j}/p_{t,\infty}=237.81$

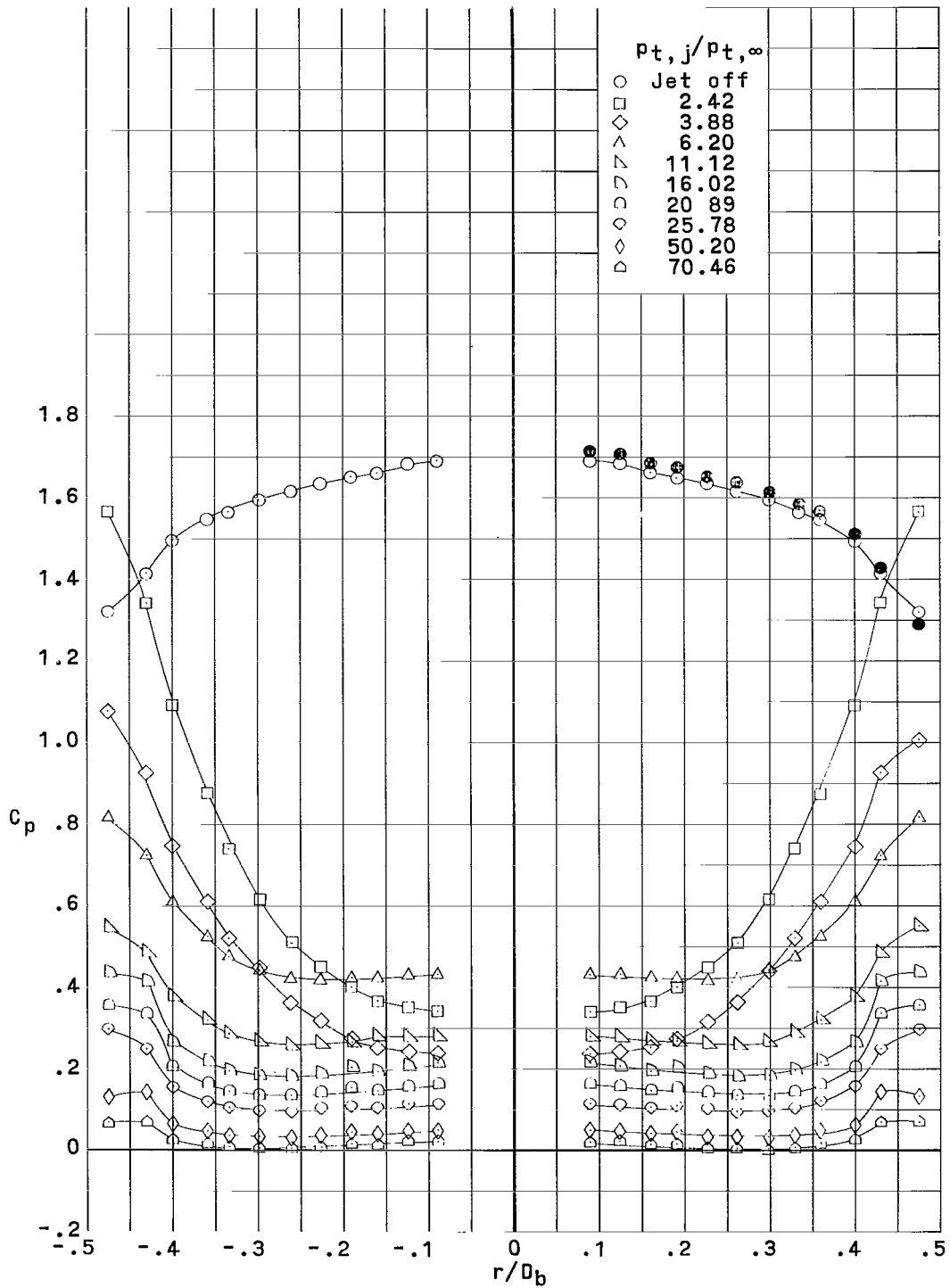


$p_{t,j}/p_{t,\infty}=246.09$

(f) Schlieren photographs at $\alpha = 5^\circ$.

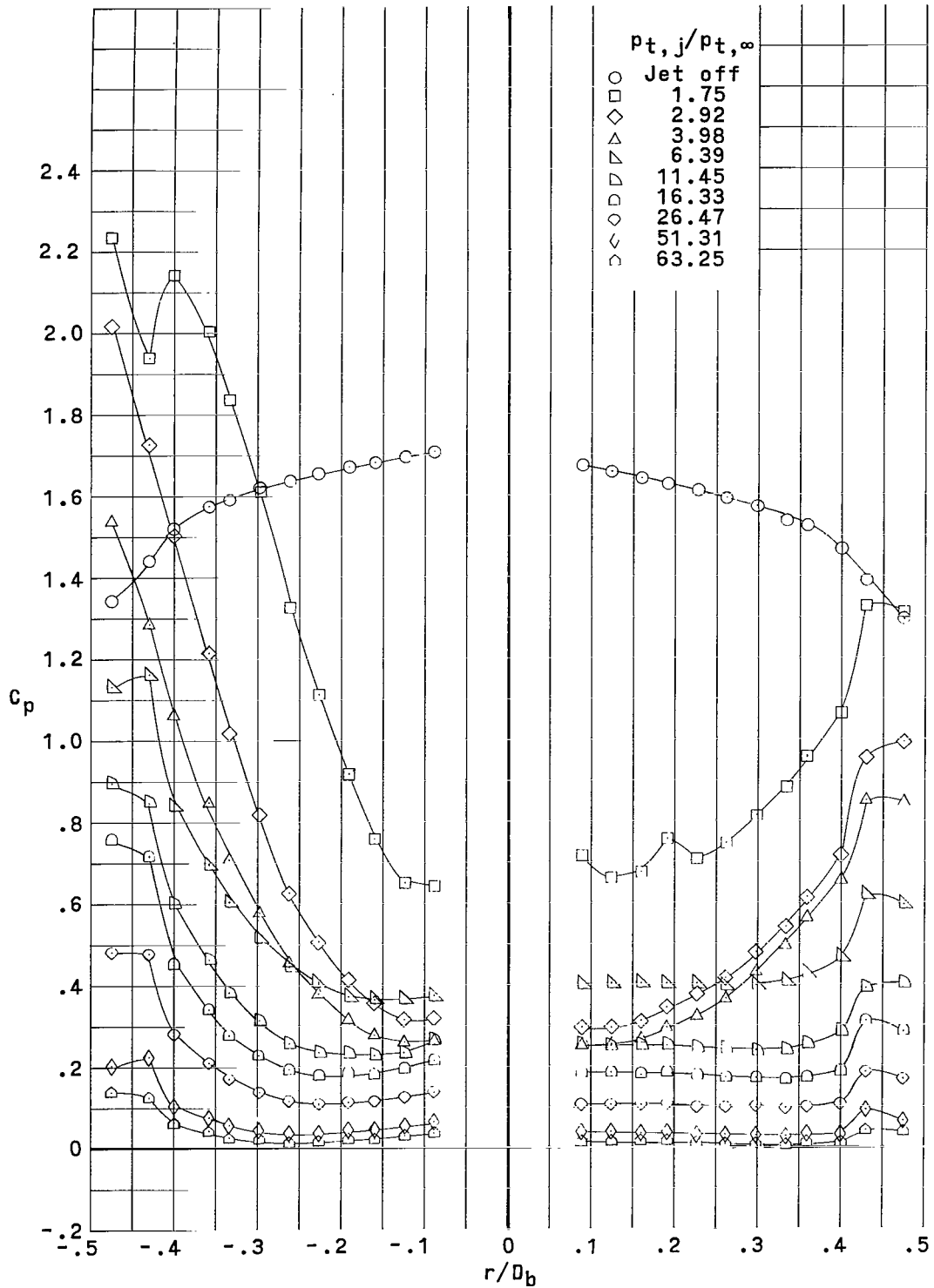
L-70-4749

Figure 3.- Concluded.



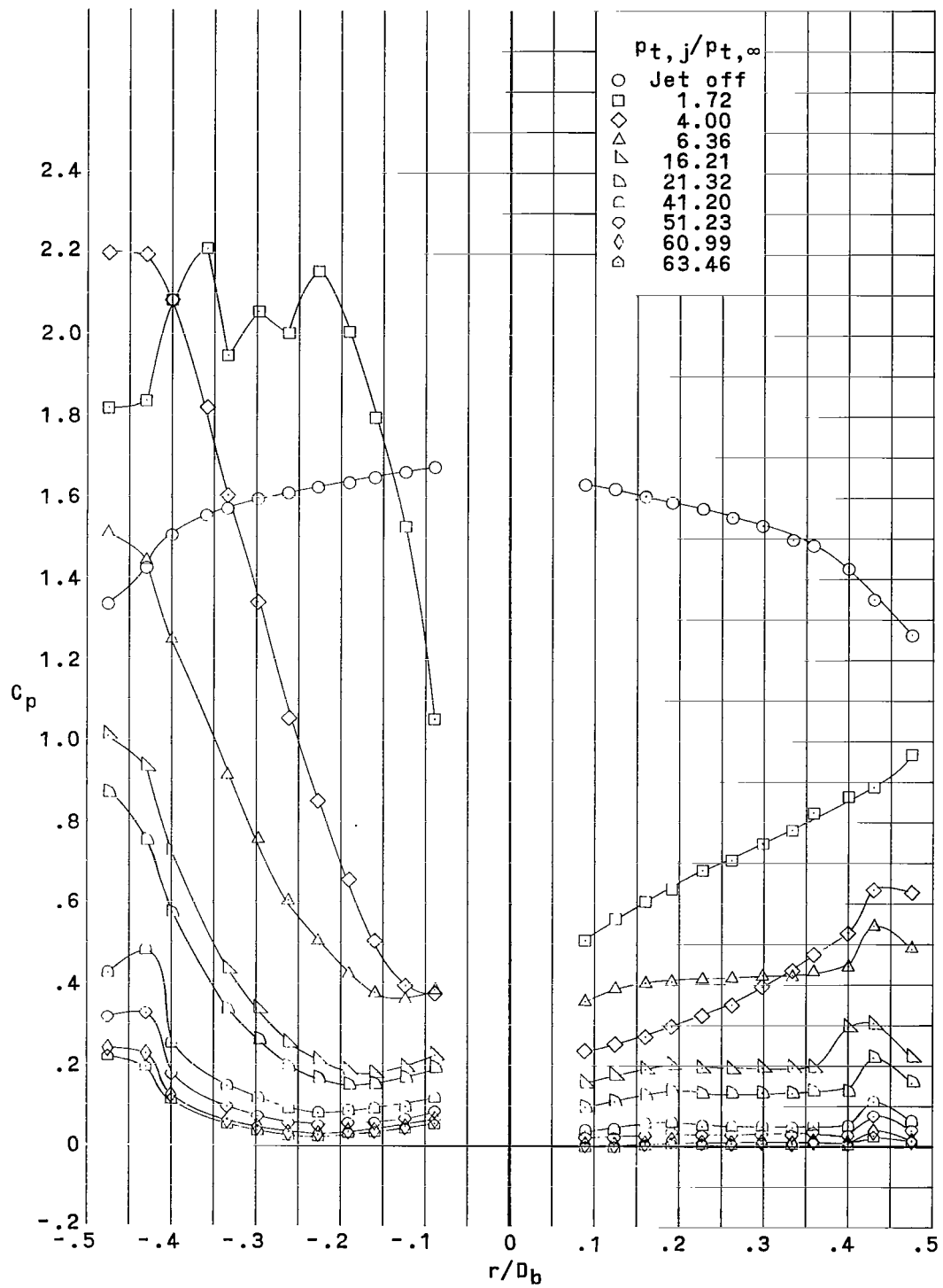
(a) Pressure distribution at $\alpha = 0^\circ$.

Figure 4.- Pressure distributions and schlieren photographs for varying $P_{t,j}/P_{t,\infty}$. $M_\infty = 4.50$. (Solid symbols indicate repeat data.)



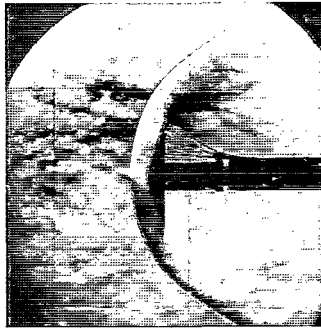
(b) Pressure distribution at $\alpha = 2^\circ$.

Figure 4.- Continued.

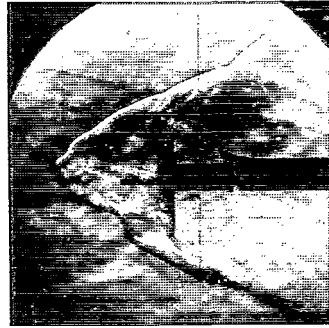


(c) Pressure distribution at $\alpha = 5^\circ$.

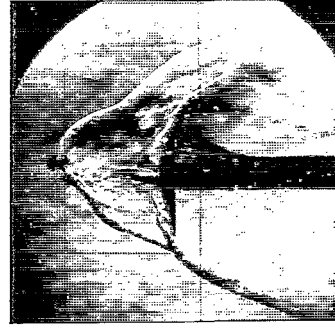
Figure 4.- Continued.



Jet off



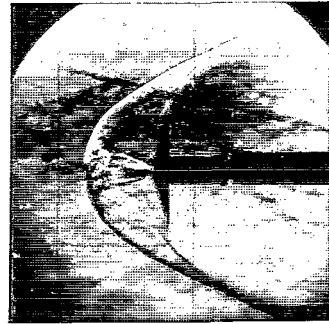
$p_{t,j}/p_{t,\infty}=2.42$



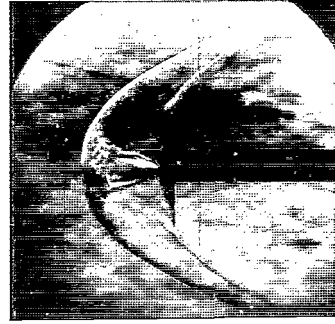
$p_{t,j}/p_{t,\infty}=3.88$



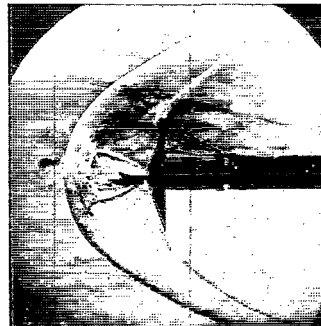
$p_{t,j}/p_{t,\infty}=6.20$



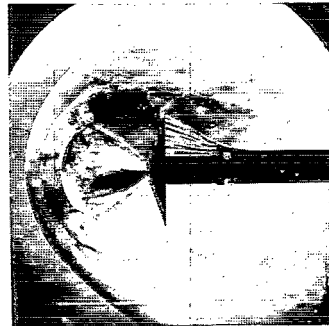
$p_{t,j}/p_{t,\infty}=11.12$



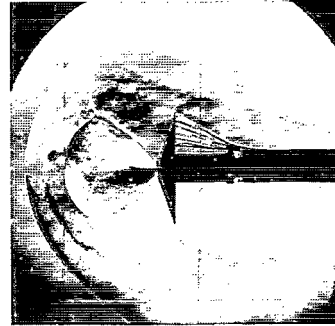
$p_{t,j}/p_{t,\infty}=16.02$



$p_{t,j}/p_{t,\infty}=20.89$



$p_{t,j}/p_{t,\infty}=50.20$

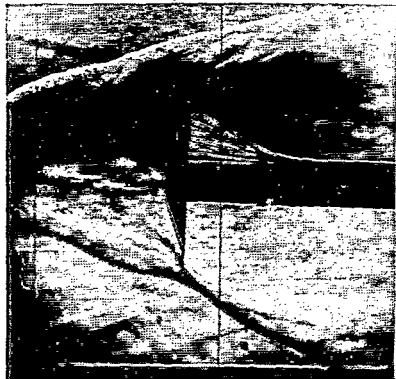


$p_{t,j}/p_{t,\infty}=59.64$

(d) Schlieren photographs at $\alpha = 0^\circ$.

L-70-4750

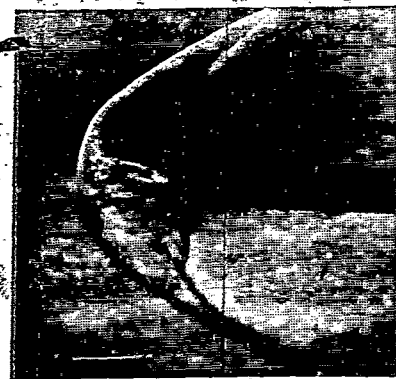
Figure 4.- Continued.



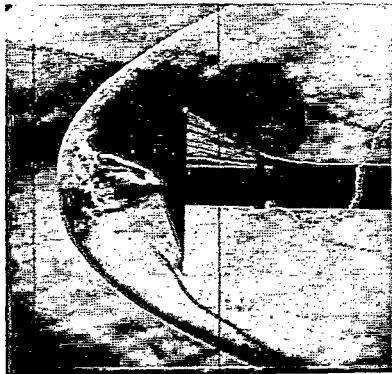
$p_{t,j}/p_{t,\infty}=3.98$



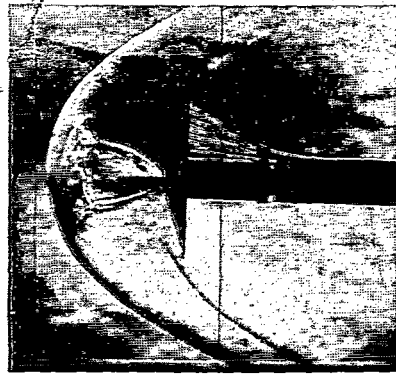
$p_{t,j}/p_{t,\infty}=6.39$



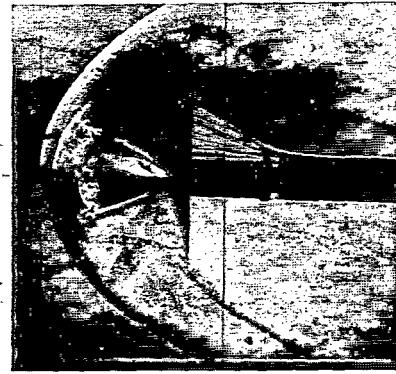
$p_{t,j}/p_{t,\infty}=11.45$



$p_{t,j}/p_{t,\infty}=21.64$



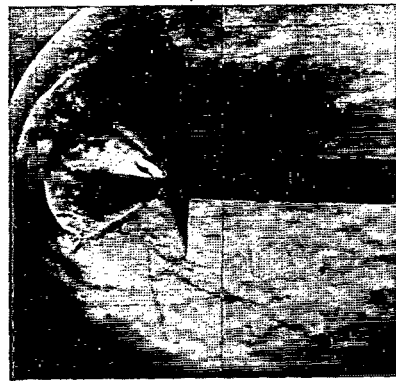
$p_{t,j}/p_{t,\infty}=26.47$



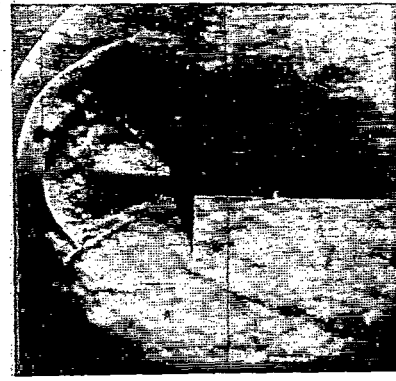
$p_{t,j}/p_{t,\infty}=41.15$



$p_{t,j}/p_{t,\infty}=51.31$



$p_{t,j}/p_{t,\infty}=61.12$

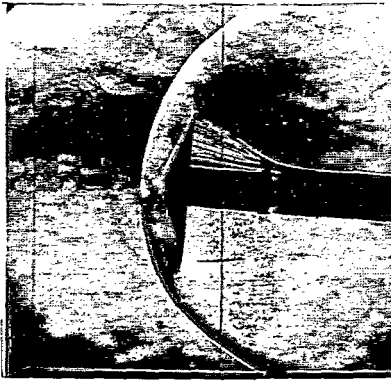


$p_{t,j}/p_{t,\infty}=63.25$

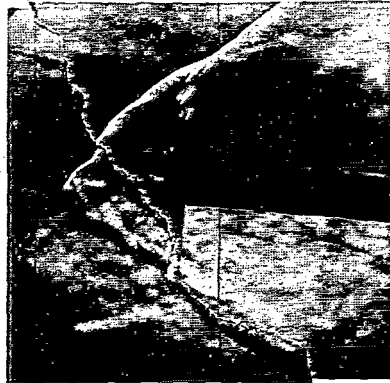
(e) Schlieren photographs at $\alpha = 2^\circ$.

L-70-4751

Figure 4.- Continued.



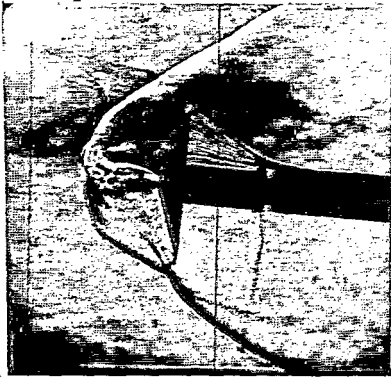
Jet off



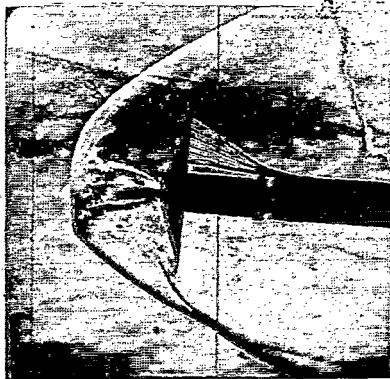
$P_{t,j}/P_{t,\infty}=1.72$



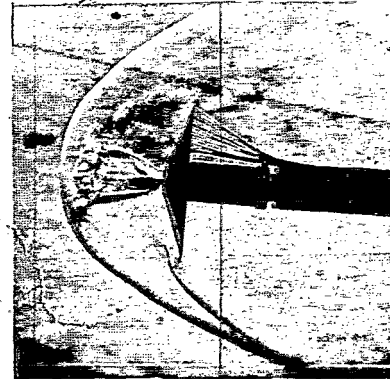
$P_{t,j}/P_{t,\infty}=2.95$



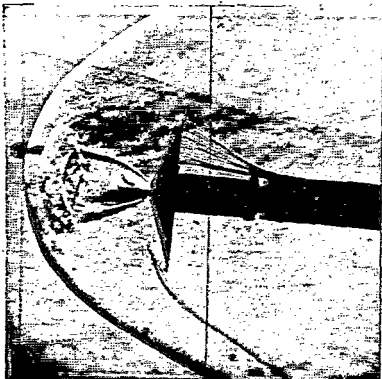
$P_{t,j}/P_{t,\infty}=6.36$



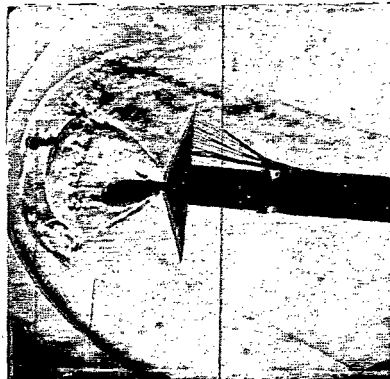
$P_{t,j}/P_{t,\infty}=11.54$



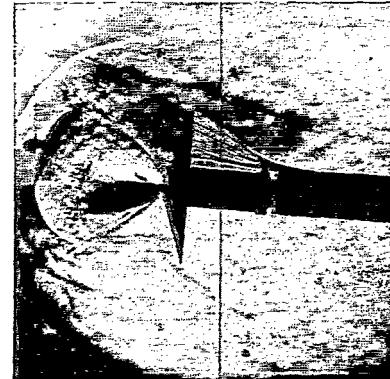
$P_{t,j}/P_{t,\infty}=16.21$



$P_{t,j}/P_{t,\infty}=26.44$



$P_{t,j}/P_{t,\infty}=51.23$

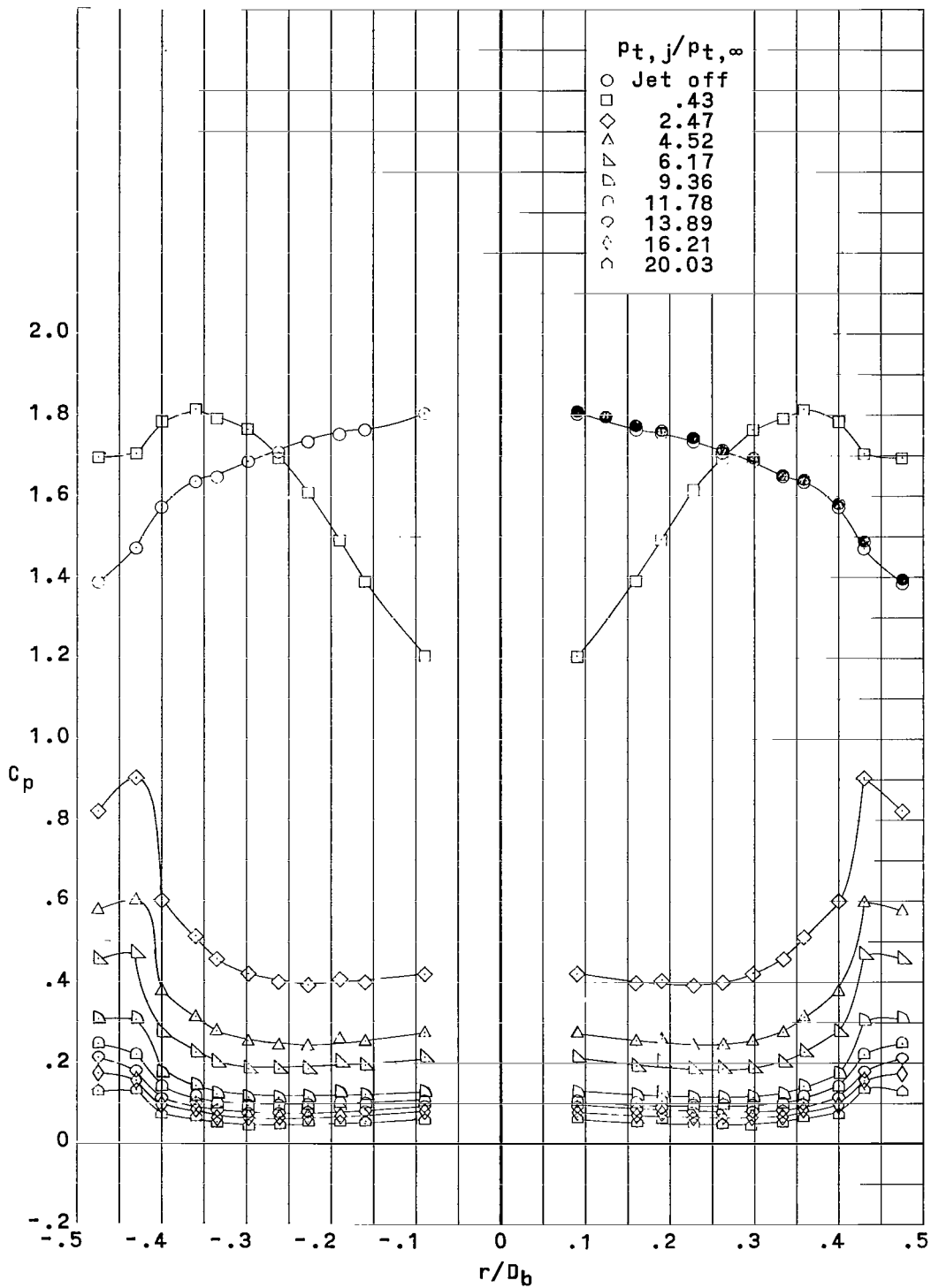


$P_{t,j}/P_{t,\infty}=63.46$

(f) Schlieren photographs at $\alpha = 5^\circ$.

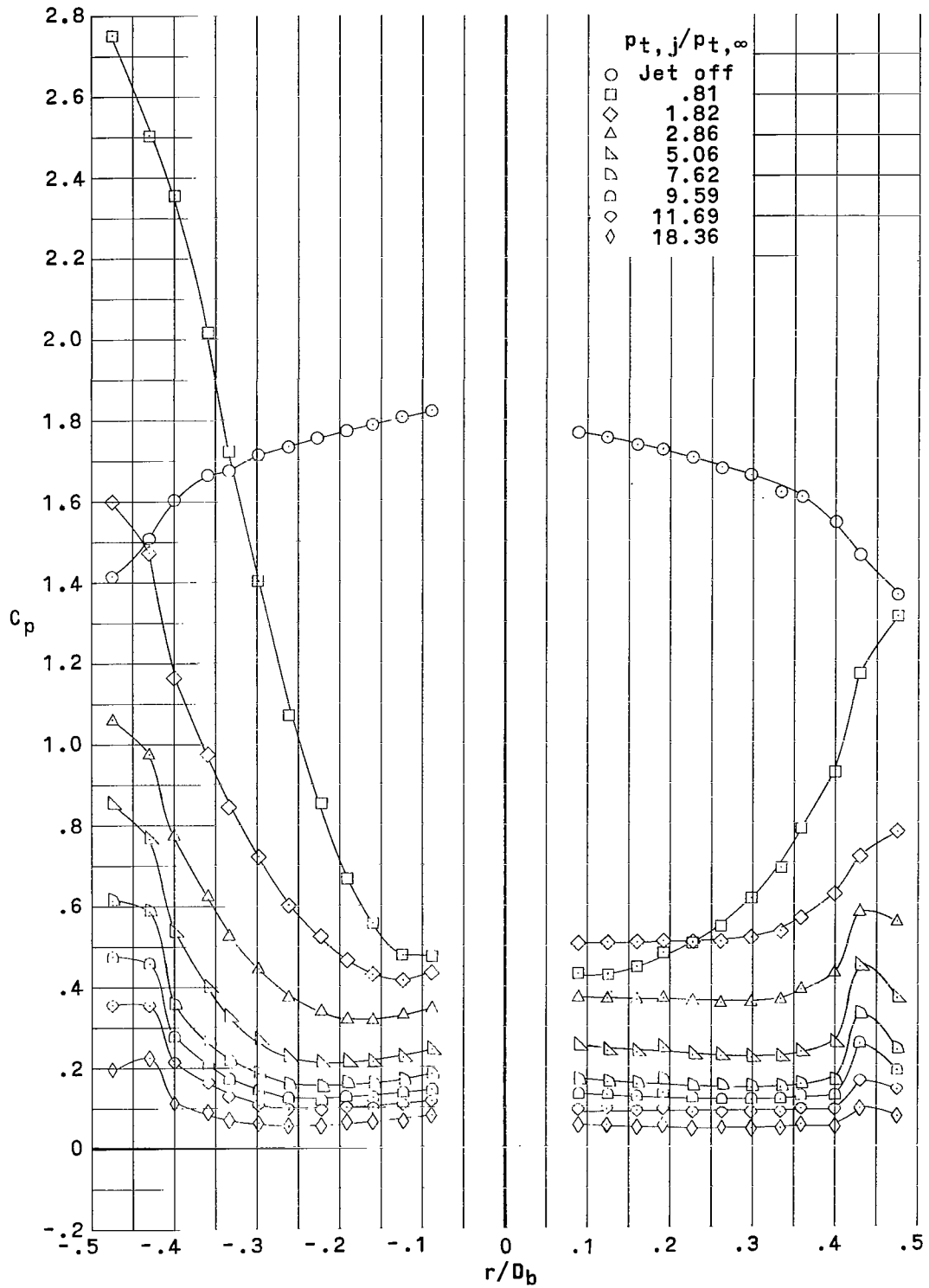
L-70-4752

Figure 4.- Concluded.



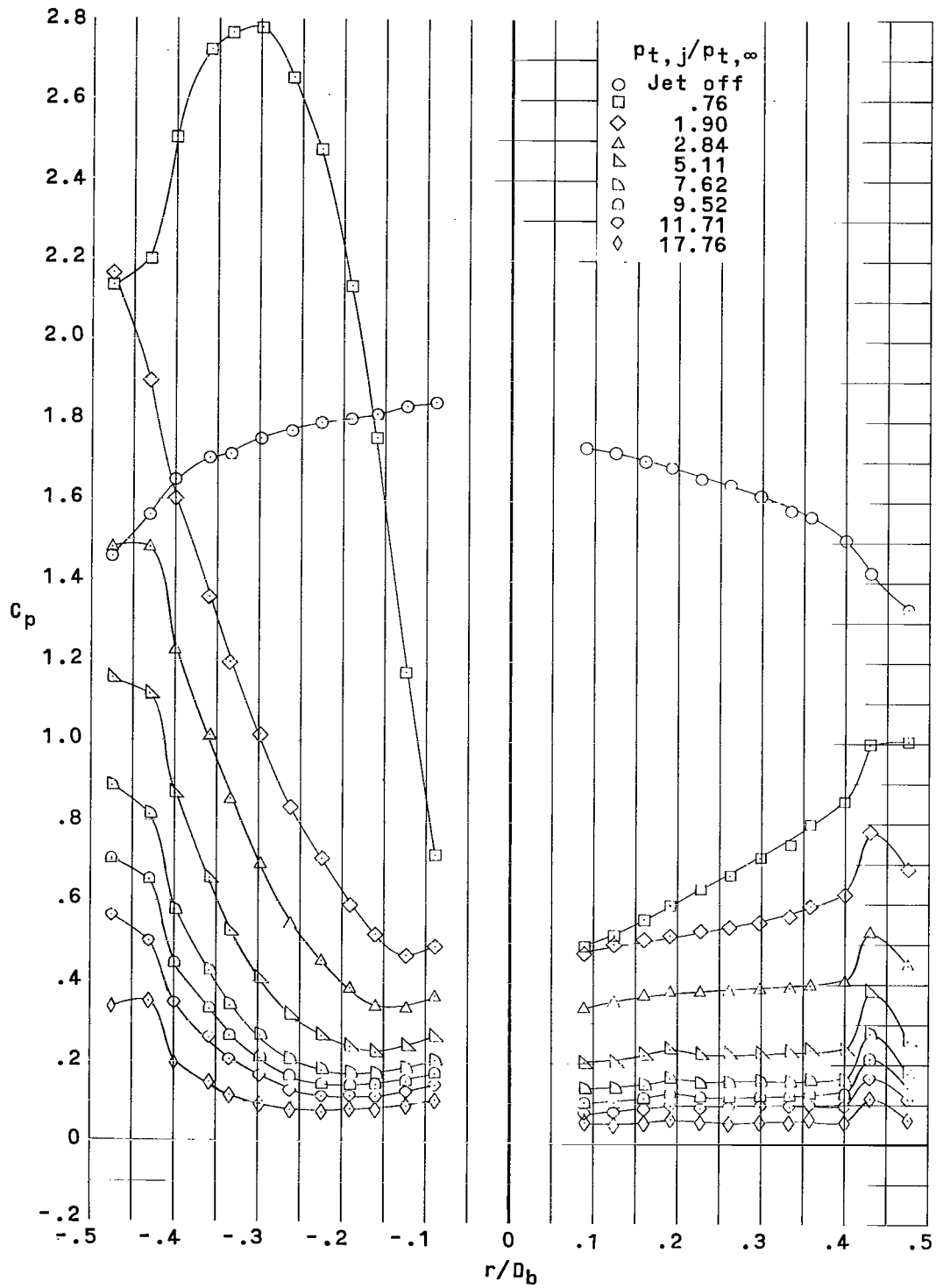
(a) Pressure distribution at $\alpha = 0^\circ$.

Figure 5.- Pressure distributions and schlieren photographs for varying $p_{t,j}/p_{t,\infty}$. $M_\infty = 6.00$. (Solid symbols indicate repeat data.)



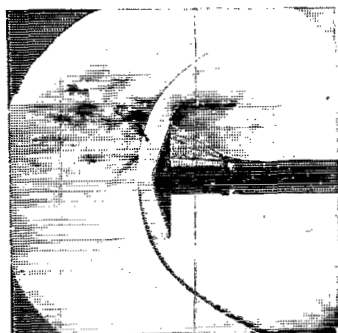
(b) Pressure distribution at $\alpha = 2^\circ$.

Figure 5.- Continued.

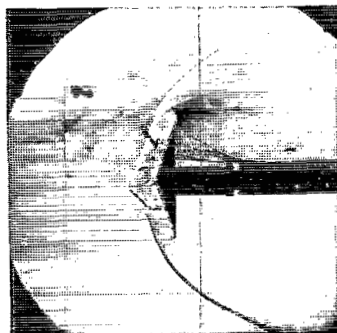


(c) Pressure distribution at $\alpha = 5^\circ$.

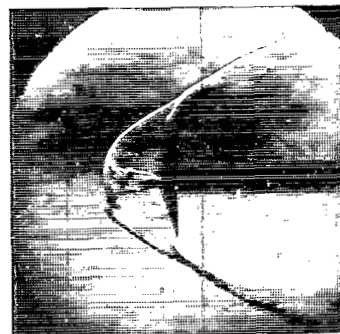
Figure 5.- Continued.



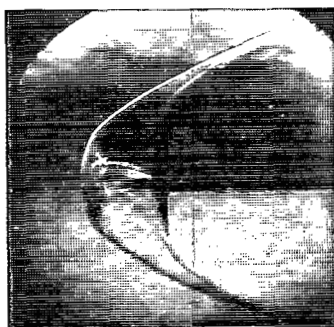
Jet off



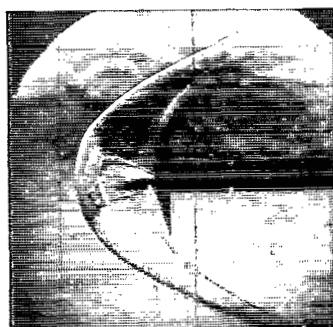
$P_{t,j}/P_{t,\infty}=0.43$



$P_{t,j}/P_{t,\infty}=2.47$



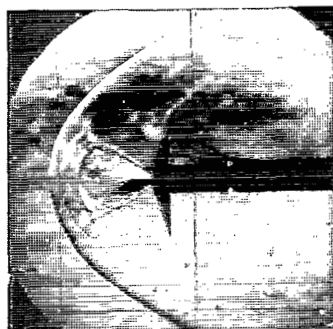
$P_{t,j}/P_{t,\infty}=4.52$



$P_{t,j}/P_{t,\infty}=6.17$



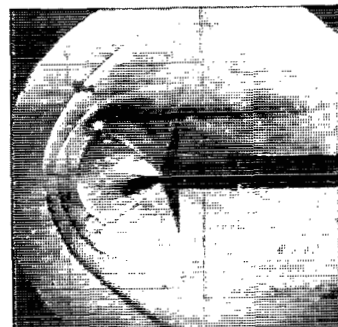
$P_{t,j}/P_{t,\infty}=9.36$



$P_{t,j}/P_{t,\infty}=11.78$



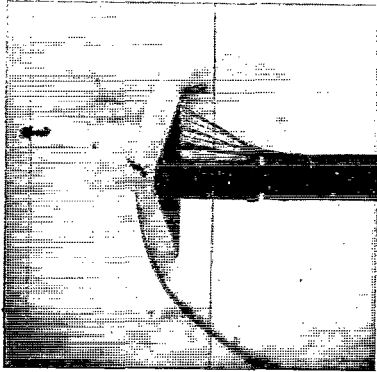
$P_{t,j}/P_{t,\infty}=13.89$



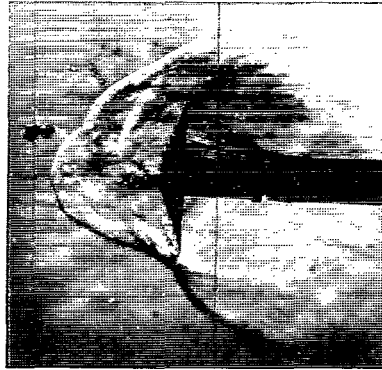
$P_{t,j}/P_{t,\infty}=16.21$

(d) Schlieren photographs at $\alpha = 0^\circ$. L-70-4753

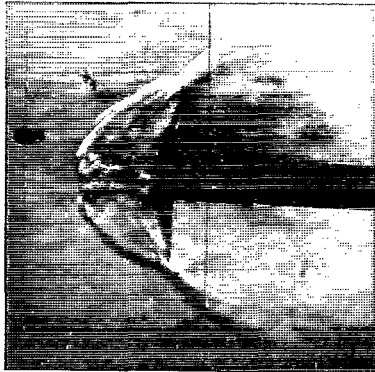
Figure 5.- Continued.



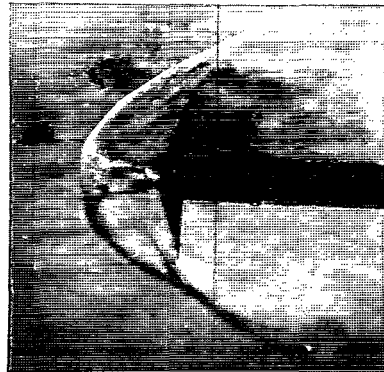
Jet off



$p_{t,j}/p_{t,\infty}=0.81$



$p_{t,j}/p_{t,\infty}=1.82$



$p_{t,j}/p_{t,\infty}=2.86$

L-70-4754

(e) Schlieren photographs at $\alpha = 2^\circ$.

Figure 5.- Concluded.

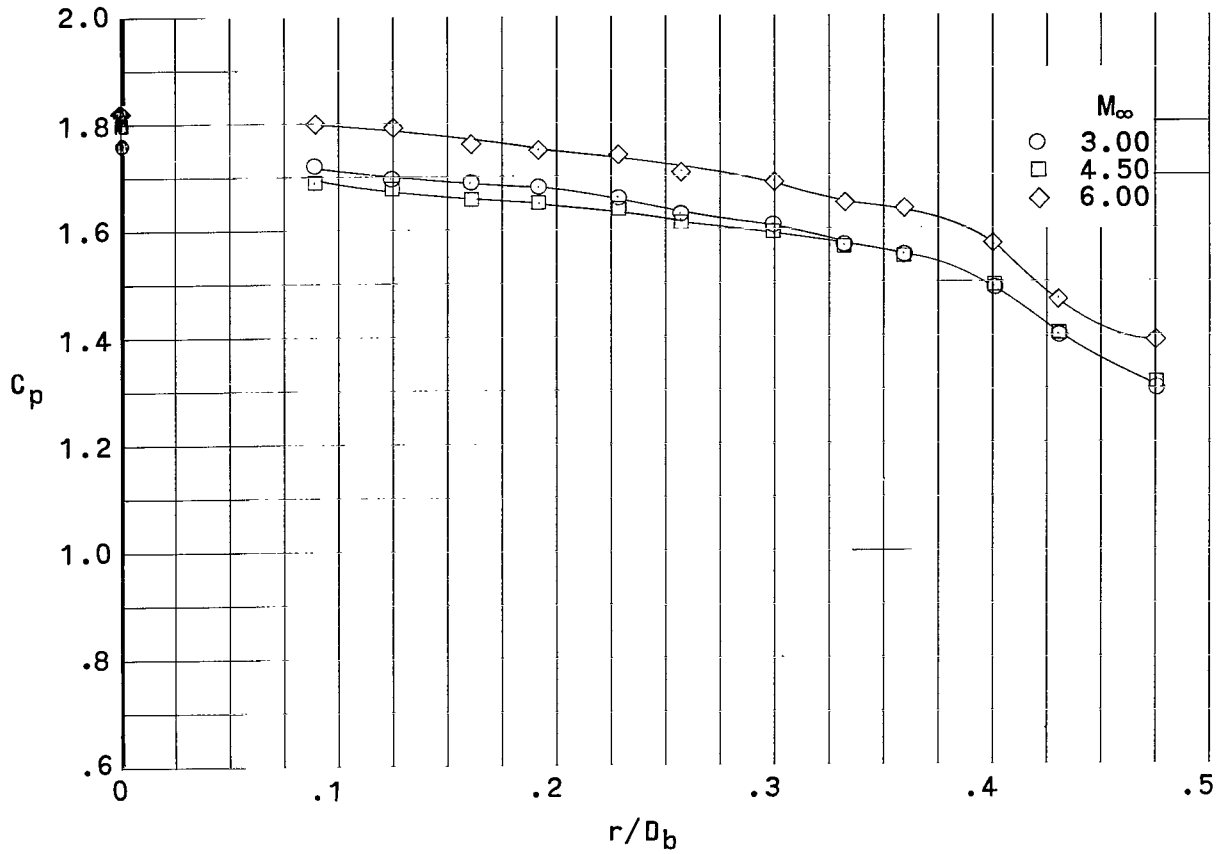


Figure 6.- Effect of Mach number on pressure distributions. Jet off; $\alpha = 0^\circ$.
 (Solid symbols denote calculated values of C_p for normal shock.)

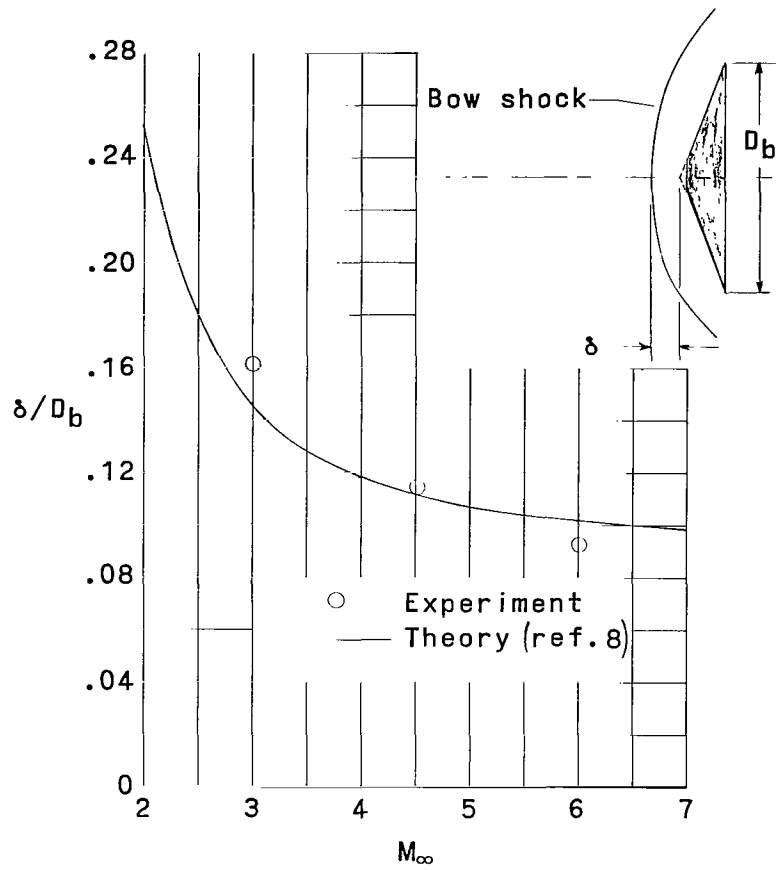
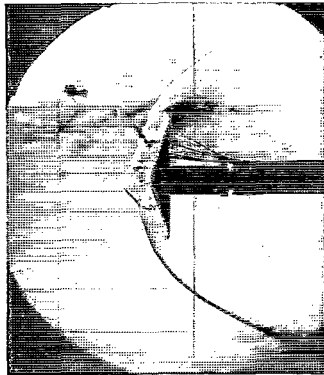
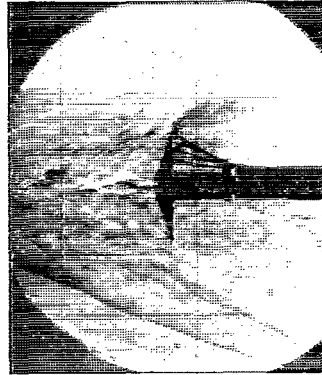


Figure 7.- Bow-shock standoff distance as a function of Mach number. Jet off; $\alpha = 0^\circ$.



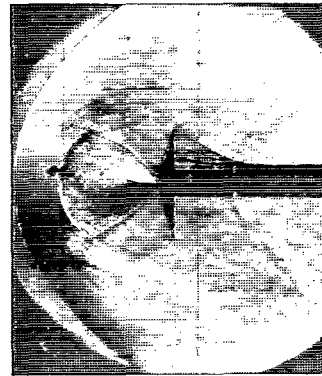
Regime 1
Unsteady
 $C_T=0.03$
 $p_j < p_s$



Regime 2
Unsteady
 $C_T=0.11$
 $p_j \approx p_s$



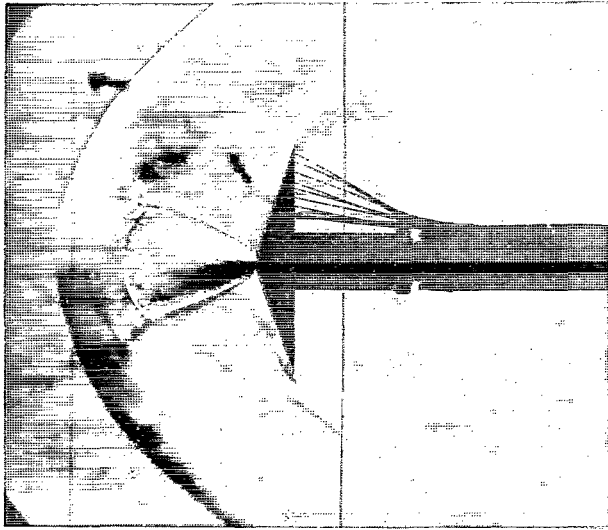
Regime 3
Steady
 $C_T=0.32$
 $p_j > p_s$



Regime 4
Steady
 $C_T=1.60$
 $p_j > p_s$

L-70-4755

Figure 8.- Typical schlieren photographs which illustrate the flow regimes that occurred. $\alpha = 0^\circ$.



L-70-4756

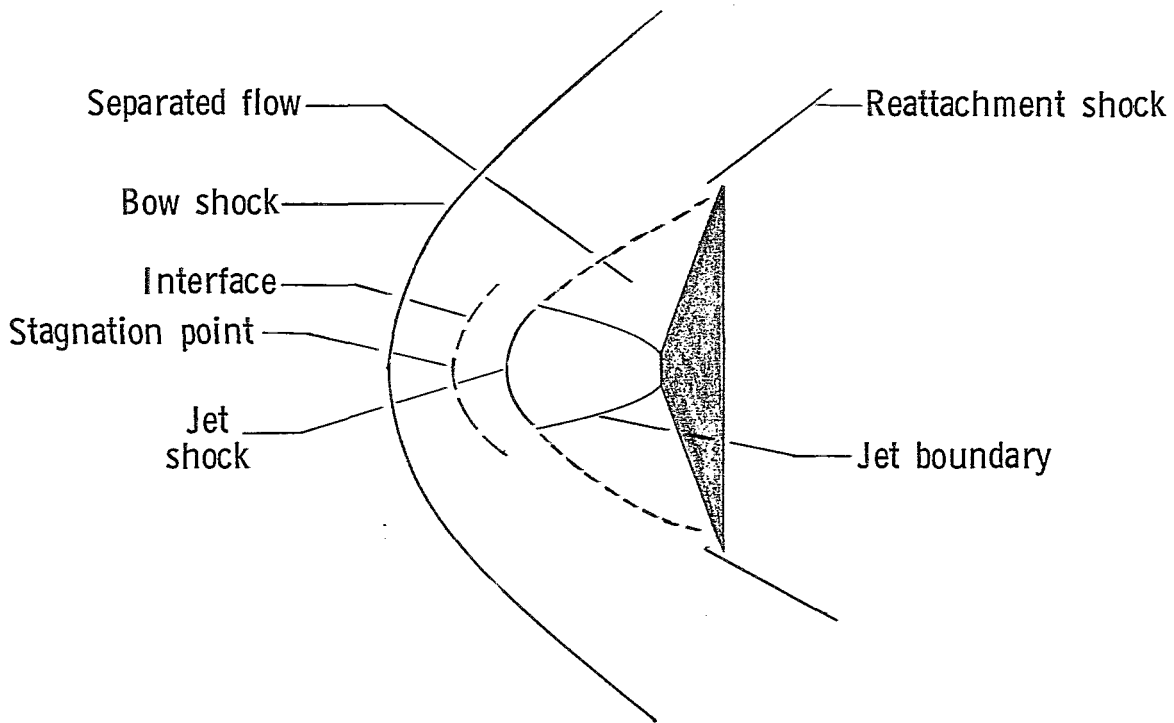


Figure 9.- Flow phenomena induced by jet. Regime 3; $\alpha = 0^\circ$.

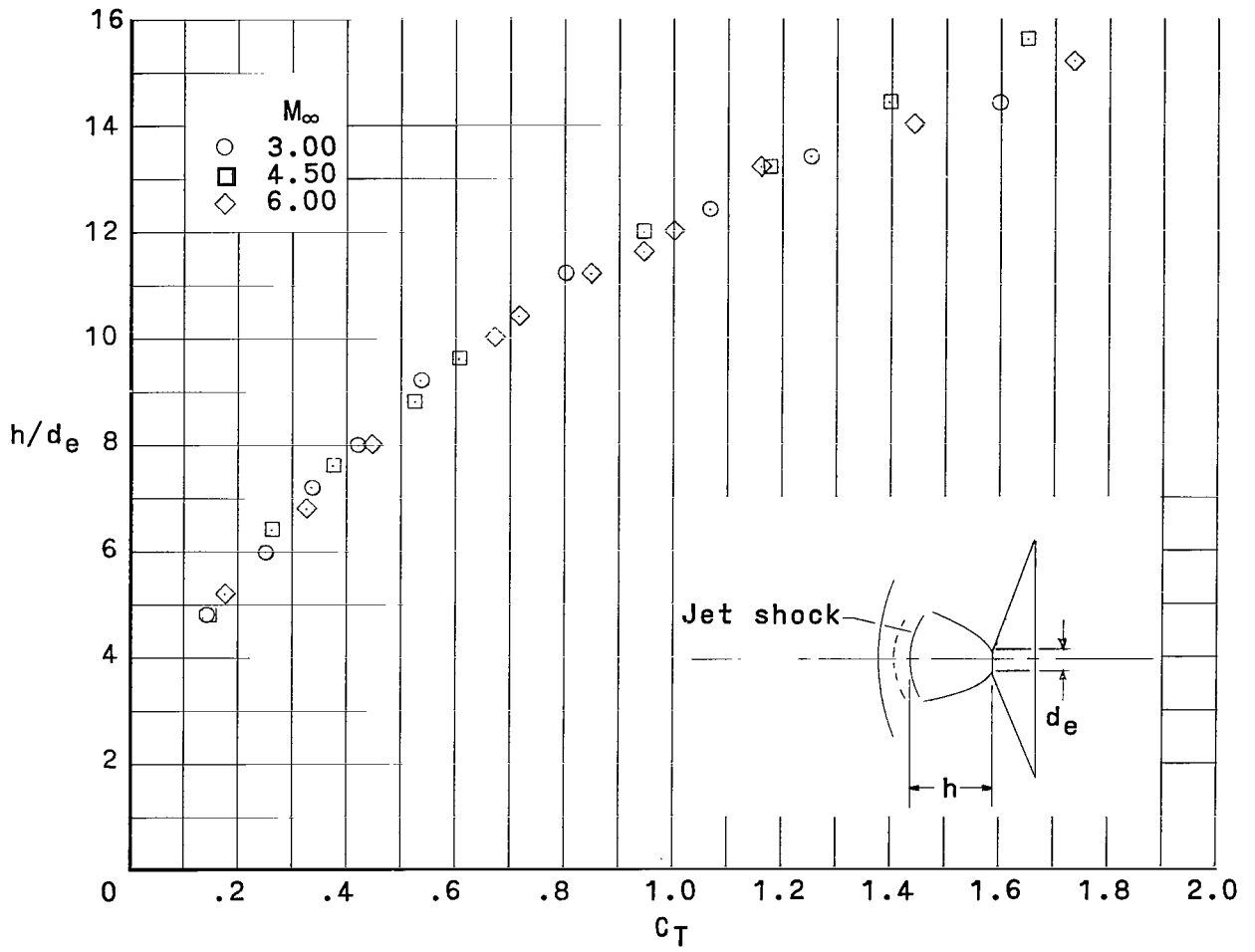


Figure 10.- Jet-shock location as a function of thrust coefficient. $\alpha = 0^\circ$.

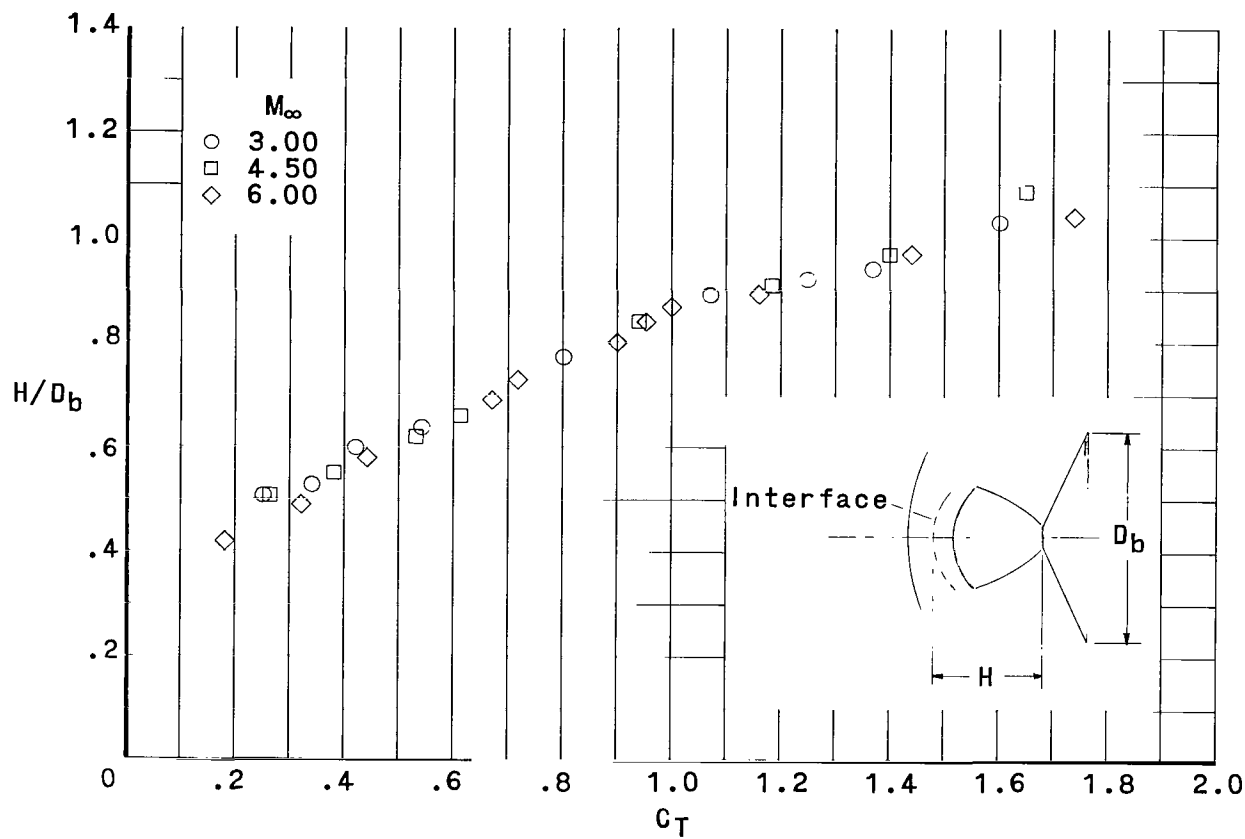


Figure 11.- Flow-interface location as a function of thrust coefficient. $\alpha = 0^\circ$.

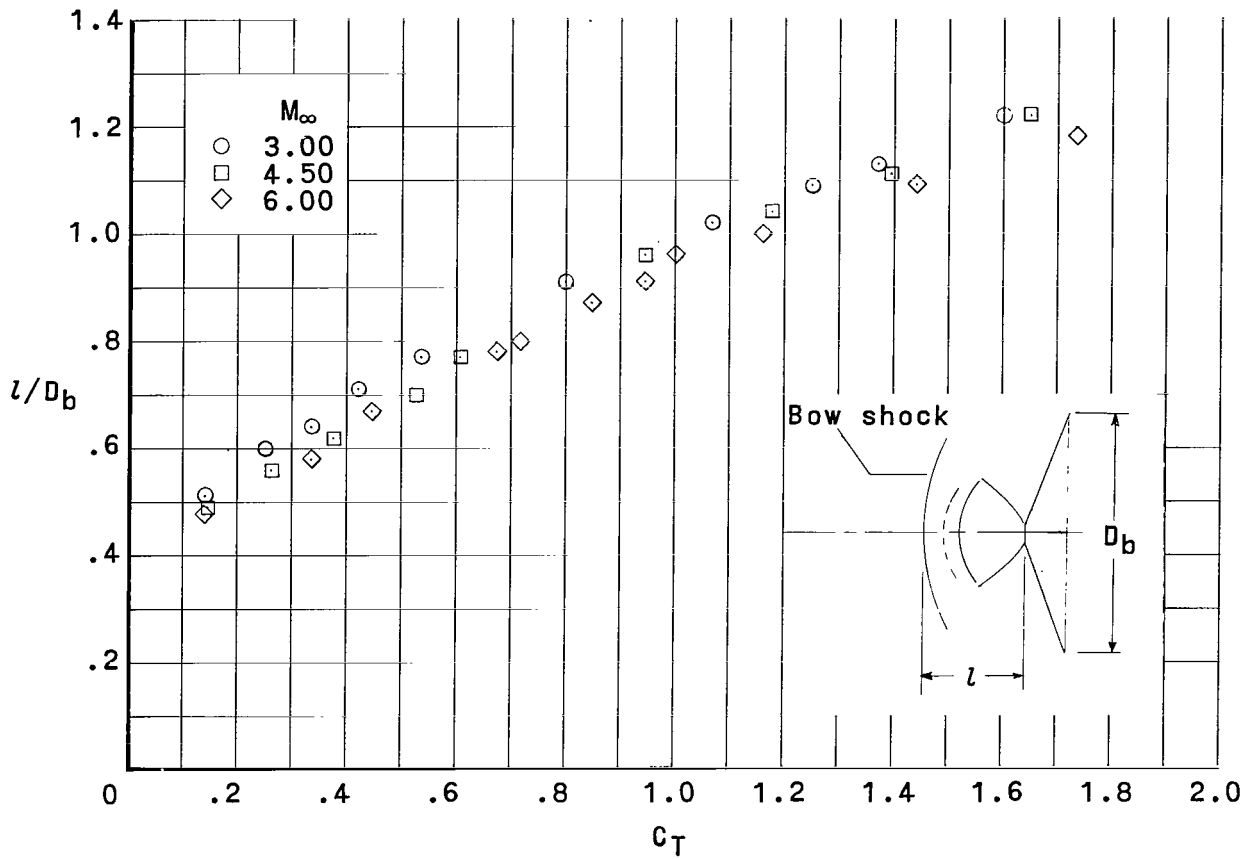


Figure 12.- Bow-shock location as a function of thrust coefficient. $\alpha = 0^\circ$.

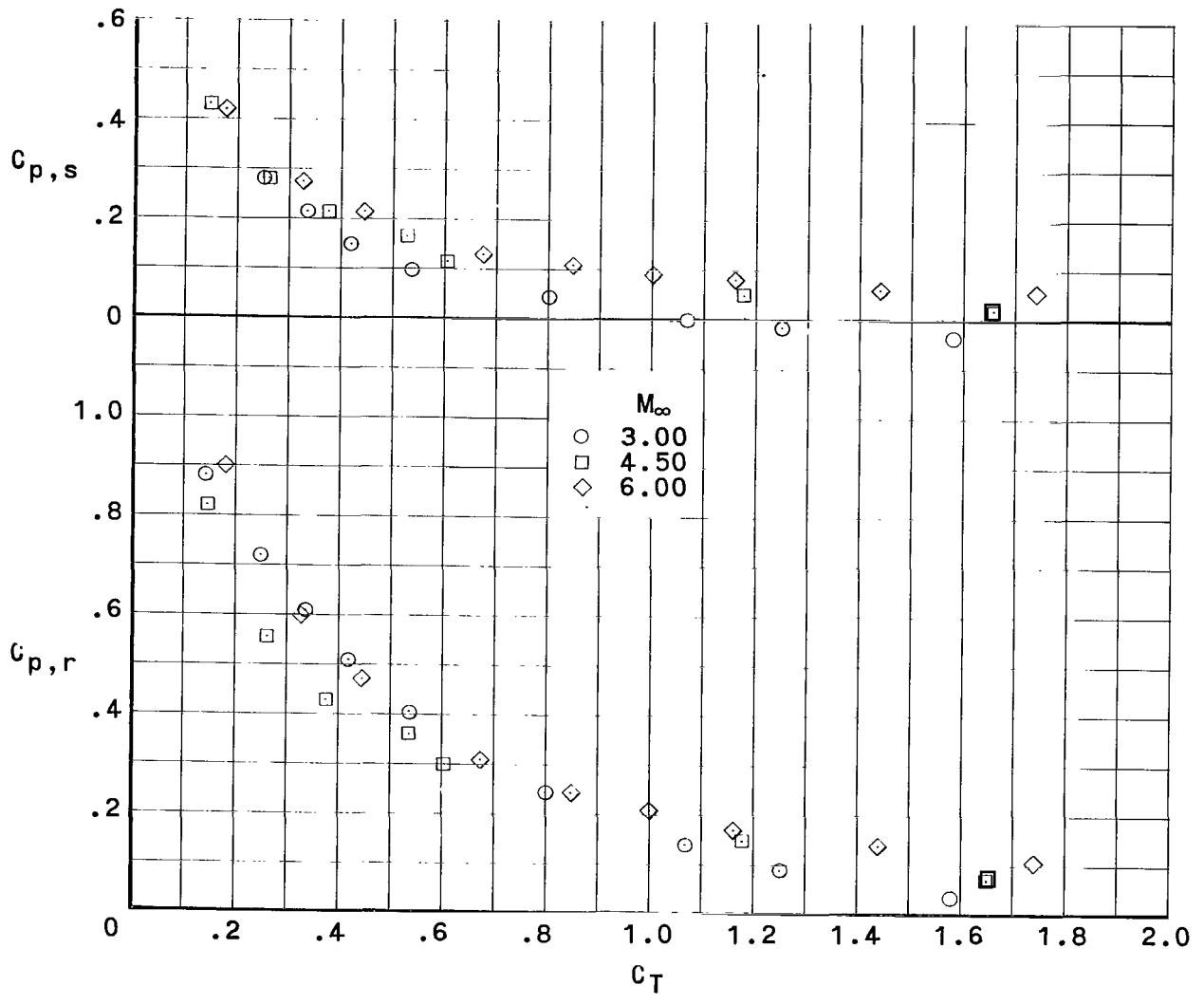


Figure 13.- Pressure coefficients at separation and reattachment as functions of thrust coefficient. $\alpha = 0^\circ$.

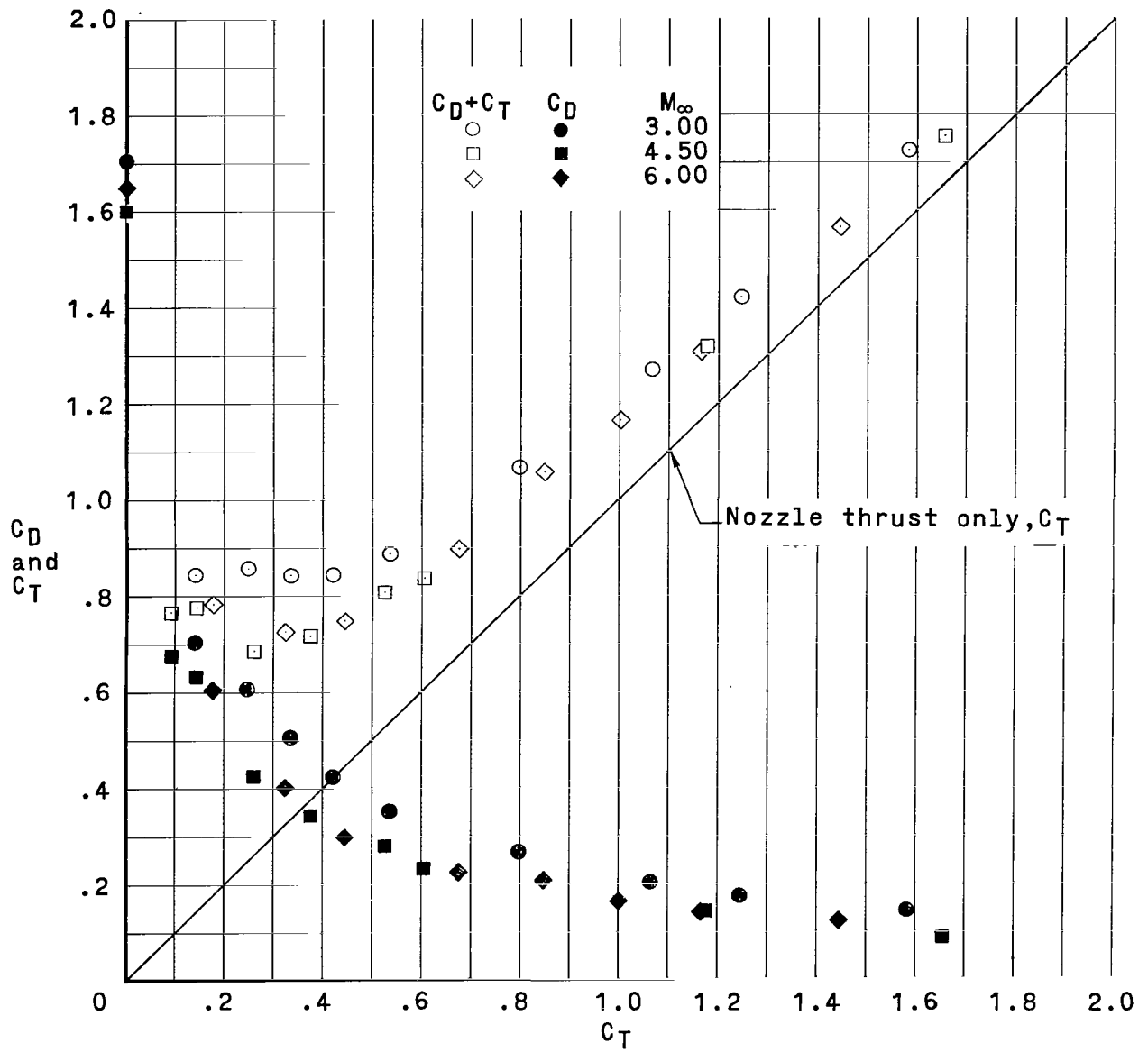
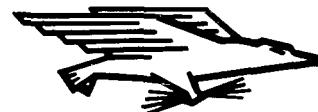


Figure 14.- Effect of retrothrust on the integrated-pressure drag coefficient. $\alpha = 0^\circ$.

FIRST CLASS MAIL



POSTAGE AND FEES PAID
NATIONAL AERONAUTICS AND
SPACE ADMINISTRATION

08U 001 26 51 3DS 71012 00903
AIR FORCE WEAPONS LABORATORY /WLOL/
KIRTLAND AFB, NEW MEXICO 87117

ATT E. LOU BOWMAN, CHIEF, TECH. LIBRARY

POSTMASTER: If Undeliverable (Section 158
Postal Manual) Do Not Return

"The aeronautical and space activities of the United States shall be conducted so as to contribute . . . to the expansion of human knowledge of phenomena in the atmosphere and space. The Administration shall provide for the widest practicable and appropriate dissemination of information concerning its activities and the results thereof."

— NATIONAL AERONAUTICS AND SPACE ACT OF 1958

NASA SCIENTIFIC AND TECHNICAL PUBLICATIONS

TECHNICAL REPORTS: Scientific and technical information considered important, complete, and a lasting contribution to existing knowledge.

TECHNICAL NOTES: Information less broad in scope but nevertheless of importance as a contribution to existing knowledge.

TECHNICAL MEMORANDUMS: Information receiving limited distribution because of preliminary data, security classification, or other reasons.

CONTRACTOR REPORTS: Scientific and technical information generated under a NASA contract or grant and considered an important contribution to existing knowledge.

TECHNICAL TRANSLATIONS: Information published in a foreign language considered to merit NASA distribution in English.

SPECIAL PUBLICATIONS: Information derived from or of value to NASA activities. Publications include conference proceedings, monographs, data compilations, handbooks, sourcebooks, and special bibliographies.

TECHNOLOGY UTILIZATION PUBLICATIONS: Information on technology used by NASA that may be of particular interest in commercial and other non-aerospace applications. Publications include Tech Briefs, Technology Utilization Reports and Technology Surveys.

Details on the availability of these publications may be obtained from:

**SCIENTIFIC AND TECHNICAL INFORMATION OFFICE
NATIONAL AERONAUTICS AND SPACE ADMINISTRATION
Washington, D.C. 20546**